

Heterogeneous Particles with Isotropic
Interactions: Investigating the Effect of Multiple
Species and Particle Size Disparity on
Self-Assembly

by
Shawn Dion

A thesis
presented to the University of Waterloo
in fulfilment of the
thesis requirement for the degree of
Masters of Science
in
Physics

Waterloo, Ontario, Canada, 2015
©Shawn Dion 2015

I hereby declare that I am the sole author of this thesis. This is a true copy of the thesis, including any required final revisions, as accepted by my examiners.

I understand that my thesis may be made electronically available to the public.

Abstract

There is much interest in using self-assembly to build materials at the microscopic level by using soft matter systems such as block copolymers and DNA coated colloids. Self-consistent field theory (SCFT) has seen much success in examining the equilibrium structure of polymer systems. We have designed a model using SCFT that describes a system of isotropically interacting particles. This model can be used a starting point to exploring different types of soft matter systems that exhibit self-assembly. This approach is a quick and efficient approach to finding equilibrium structures, and can be used as a high throughput method for finding equilibrium structures. We present here two different systems: a triblock star polymer and a colloidal system. We show that our approach, while extremely coarse grained can replicate the robust phases of those systems. In the triblock copolymer system we can show that the honeycomb lattice phase, the lamella phase and the lamella with beads phase are easily obtained. We compare the phases found in our model to the most common phases found using SCFT for polymers systems. In the colloidal system, we can replicate some of properties of a large colloidal particle surrounded by a solution of much smaller solution particles.

Acknowledgements

I would like to thank Dr. Russell Thompson and my peer Kier von Konigslow for the insightful discussions.

Contents

Abstract	iii
Acknowledgements	iv
Contents	v
List of Figures	vii
Abbreviations	viii
1 Introduction	1
1.1 Motivation	1
1.2 Brief Overview	3
2 Background	6
2.1 Polymer Systems	7
2.1.1 Linear and Miktoarm Copolymers	7
2.1.2 Self Consistent Field Theory as Applied to Polymer Systems	9
2.2 Colloidal Nano-Particles	14
2.2.1 Modelling For Self-Assembling DNA Colloids	16
3 Theory	19
3.1 Phase Separation	19
3.2 N Particles with Isotropic Interactions	20
3.2.1 Hamiltonian	20
3.2.2 Partition Function	23
3.2.3 Potential	30
3.2.4 Computation of SCFT equations	32
3.2.4.1 Computational Approach	33
3.2.4.2 Fourier Transforms and Convolutions	34
3.2.4.3 Computation Parameters	35
3.2.4.4 Algorithm	36
3.3 Two Species of Particles with Large Particle Disparity	37
3.3.1 Issues with SCFT and Particle Size	37
3.3.2 Derivation of a New Fixed Point Equation	38

3.3.3	Computation	40
3.3.3.1	Fixed Point Equations	40
3.3.3.2	Calculating Equilibrium Solutions	41
3.3.3.3	Algorithm	43
4	Results and Discussion	45
4.1	Three Species Case	45
4.1.1	Parameters	45
4.1.2	Relation to Copolymer Melts	47
4.1.3	Effect of the Length Scale	51
4.1.4	Three Dimensional Phases	53
4.1.5	Improvements and Future Work for Polymer Systems	54
4.2	Particle Disparity	55
4.2.1	Two Different Sized Particles in 1D	56
4.2.2	Two Different Sized Particles in 2D	57
4.2.3	Convergence	59
4.2.4	Improvements and Future Work for Particle Disparity	60
5	Conclusions	61
A	Appendix A. <i>Functional Integration</i>	63
	Bibliography	66

List of Figures

1.1	A schematic comparison between a particle based model and polymer based model	4
2.1	A linear triblock copolymer	8
2.2	A miktoarm or star triblock copolymer	9
2.3	Basic star triblock morphologies found using SCFT	11
2.4	A figure of various star triblock morphologies found using SCFT	12
2.5	More specific triblock morphologies found using SCFT	13
2.6	Schematic of a pair of DNA colloids	15
3.1	Plot of the isotropic interacting potential	32
4.1	Majority plots of different phases	49
4.2	Ternary plot for ABC star triblock	50
4.3	Ternary plot for ABC star triblock with a more specific search method	51
4.4	Lamella with beads using non standard volume fractions	52
4.5	3D iso-surface plots	54
4.6	1D density plot with large particle disparity	57
4.7	2D density plot with large particle disparity	58

Abbreviations

DNACC	DNA Coated Colloids
SCFT	Self-Consistent Field Theory
DFT	Density Functional Theory
FFT	Fast Fourier Transform

Chapter 1

Introduction

1.1 Motivation

Creating designer materials using self-assembly has been a long time goal for material scientists. Daan Frenkel has stated that in order to design a material at the microscopic level using self-assembly: “the target structure needs to be thermodynamically the most stable among all possible arrangements, as well as kinetically accessible under the same conditions to avoid the self-assembly process getting trapped in unwanted, metastable structures” [18]. In order to meet both those requirements, control of the material at the microscopic level is needed and would allow one to endow the material with a variety of different properties, depending on the building blocks used and the microstructures they form. There are a variety of different materials that can possibly fit this scheme, including DNA coated colloids (DNACCs) as well as block copolymers. Both of these systems have been thoroughly studied in a theoretical nature, and have been tested successfully against experiment [7, 17, 32]. There is however still much to be done: there is a large knowledge gap between what is desired in these materials and how to build them.

Block copolymers have been of much theoretical and practical interest as a means of producing engineered materials through self-assembly. Much work has been

done studying different polymer systems with field theories. Field theories are an ideal starting point to exploring other soft matter systems, including DNACCs, that might be able to undergo self-assembly. Self-consistent field theory (SCFT) has seen much success in examining diblock copolymer systems [14, 17]. It is well suited to being used to study the equilibrium phases of DNACCs as well [23, 46]. This method has the advantage of being computationally quick and efficient [37]. It also allows the computation of a variety of different phases based on the interactions between particles [42]. As a research tool this allows for an extensive exploration of the equilibrium phases, with the goal of discovering the design rules for a given system.

Over the past decade there has been much research into the viability of using DNACCs as the building blocks to engineer materials at the microscopic scale. Using the specificity of DNA base pair interactions, it is possible that a system will self assemble to a desired morphology at equilibrium. Controlling these interactions at the micrometer scale would allow one to tailor the optical or electronic properties of the materials [34]. Colloids can be mixed and matched by their properties in order to build novel materials that meet a desired set of qualifications. It is not presently possible to accurately predict what types of coatings are necessary to form any particular structures, as well as whether or not the system will even be kinetically accessible [18, 28].

DNACCs as well as block copolymers both undergo self-assembly under the right conditions and the study of the equilibrium morphologies of each of the systems would provide much insight into their real world use. SCFT is a powerful tool in studying self-assembling systems, with years of proven use in polymer systems and some success in DNACCs, it is in a unique position to study the self-assembly of these systems [10, 32]. As such, a coarse grain model in the spirit of SCFT can be used to study both DNACC's and block copolymers. A simplistic coarse grain approach using isotropic interacting particles is the ideal starting point to obtaining a SCFT description that works roughly for both DNACCs and polymer systems.

In this thesis a simple particle-based coarse grain model is presented in which the particles interact isotropically with one another. It is possible that this approach can replicate some of the phases that are found in both the polymer and colloidal systems. This approach is the lower bound of how simple a self-assembling system can be, and the phases that are found with this system will be the simplest possible. As Xu *et al.* points out [53], we can use a simple and fast algorithm to generate a large number of equilibrium structures and these results can be used to build phase diagrams. The phases found with the simple coarse grain model should be used as a starting point to find more complicated structures theoretically with a more accurate model. Finding the conditions for a simple model of phases is a good starting point to engineer these phases experimentally.

1.2 Brief Overview

Using the model developed by von Konigslow *et al.* [23, 46] as the starting point, we can generalize that model to a system of many different particles. If all the particles are held to the same parameters it is easy to imagine that the equilibrium phase would need to be invariant under the relabelling of particles. This limits the amount of different types of morphologies that one might get for that type of system. This type of system will exhibit simple phases that should be robust and stable. As one can imagine, increasing the system to even more species of particles will drastically increase the complexity of the different morphologies.

The model used by von Konigslow *et al.* [23, 46] has a system of particles that interact with each other through some predetermined potential. Through this potential the particles have a spatial extent and through this potential one can argue that this type of coarse grain model, with particles, will have some similarities with a polymer model. Figure 1.1 represents a basic schematic on how a miktoarm polymer may transfer over its basic shape over to our particle model. It is in this vein that this model can be used to examine block copolymer systems; under the right conditions the results of our coarse grain model should reflect the results of

a polymer model. There has been significant research into triblock polymer melts using SCFT, and a lot of research on the different types of phases obtainable under different conditions. We focus on the results for two dimensional phases for triblock copolymers, since these results are more plentiful than the three dimensional counter parts. We can however generate phases in three dimensions. We aim to compare the phases of the coarse grain model to the full SCFT polymer models to show that there is indeed some overlap between the two different systems.

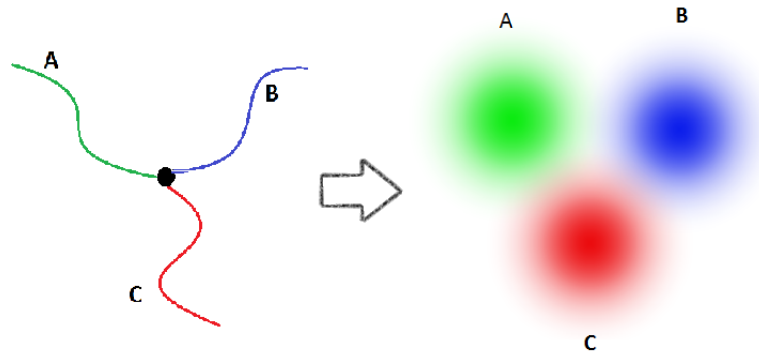


FIGURE 1.1: A Schematic comparison between particle based model and polymer based model. The polymer themselves have a basic shape but our particle model does not contain explicit information on the shape of the particles. The clouds represent a general area of influence the particles exert through the potential. It is through this potential that both system can behave similarly

Our coarse grain particle model can also be slightly modified to examine the case of two particles which differ in size by a large disparity (i.e. the size difference between a colloid and the solution). This type of change is more closely related to real world systems, and studying the affect of this on the equilibrium phases is important. This type of size disparity causes a variety of different numerical issues, but our model can be used in a limited degree to examine the equilibrium case in at least one and two dimensions. It is possible to show that some features of a system which has particle disparity are present using a field theory approach.

We hope to show the flexibility of SCFT and its modified form in this regard, by showing how a simple particle model with isotropic interactions can be used to study different types of soft matter systems in a numerically efficient manner. Since we are using SCFT, we are only interested in the equilibrium of a given system, and constructing a catalogue of the possible phases at equilibrium. We do not take into account how the equilibrium structure can be reached or if it is stable and instead focus on the first of Frenkel's design rules on how the parameters of the system effect the equilibrium. We compare our approach to ABC star triblock copolymers. The ability to specify the interactions between the particles will allow one to examine a variety of different microphase structures and we hope to show that the most robust of the structures match the triblock copolymer phases. When comparing to colloidal systems we show that this approach using isotropically interacting particles can be modified to examine a system of a colloid suspended within a solution.

Chapter 2

Background

Self-assembly is the idea that a system, without external influence, will reach a desired equilibrium state. The system will do this due to some sort of interactions between the constituents of the system. The main goal with self-assembly is being able to design materials at a microscopic level by tailoring the interactions between the building blocks of the material so that a wanted phase forms. Aside from very simple structures, our ability to control the interactions at a level in which more complicated structures would form is meagre [18]. There are two general design requirements; the target structure needs to be the most thermodynamically stable of all possible arrangements, and the system has to be able to access the structure without getting stuck in an unwanted state [18]. Focusing on the first general rule raises the question: under what conditions will a system enter a targeted stable state? Given a set of conditions on a system, what does the thermodynamically stable morphology look like?

Self-consistent field theory is an important tool in the research of self-assembling systems. SCFT is used on systems that have many different constituents that interact with each other. This is done by replacing the many body effects of all the particles on a single particle with an averaged field on the same particle. This turns a many body system into an effective one body problem. SCFT is a mean field theory that can be viewed as a saddle point approximation to the partition function [17]. Since designing materials using self-assembly inherently means that

we are using the equilibrium points to design our material, SCFT is well positioned to study the equilibrium points that can be obtained.

Two fields which show promise in the area of designer materials are: diblock, triblock and higher polymer systems, and colloidal systems, both DNA covered, and polymer covered as well. It is important to look at the successes of using SCFT in both of these systems, and to see the merit of using SCFT for a variety of different soft matter systems.

2.1 Polymer Systems

2.1.1 Linear and Miktoarm Copolymers

It is well known that block copolymer systems will undergo some level of self-assembly [17, 29, 37, 44], given the right conditions. If a polymer chain only has one type of monomer in it, it is known as a homopolymer. If two or more different types of monomers are used then the polymer chain becomes a copolymer chain, and if multiple monomers are used in a “block”, all A polymers on one side and all B polymers on the other, then these polymers are called block copolymers. Of course three different types of monomers can be used, and these monomers would form what is called a triblock copolymer system. A linear ABC triblock (figure 2.1) is when three different types of monomers are connected in an end to end chain from one end to another.



FIGURE 2.1: This is a schematic of a linear ABC triblock copolymer. The polymers are connected end to end. The three colors represent different monomers.

A miktoarm or star shaped polymer (figure 2.2), is one in which all the polymer segments are attached at one end. In most mean field theories the interactions between polymers are binary and, when the polymers are in contact there is a force, when they are not in contact there is no interaction. In a linear ABC triblock the A and C polymers do not interact as much. In a ABC miktoarm they are attached at one end; thus they all feel an interaction. For this reason we choose to focus more on miktoarm polymers, as a comparison point between this particle based system and the polymer system, since in the particle based system the interactions are chosen for simplicity to be between all particles of different types.

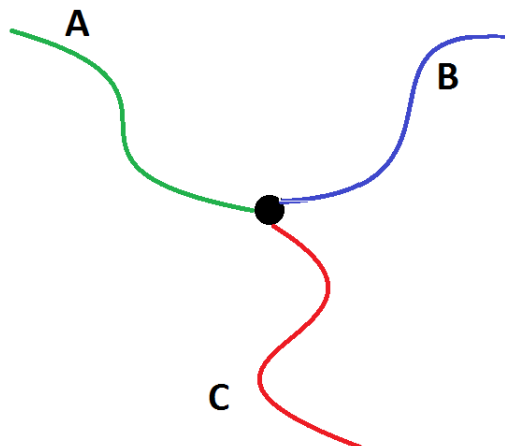


FIGURE 2.2: A schematic of a simple ABC miktoarm (star shaped) polymer. The colors represent the different polymer types ABC and the polymers are connected at one end.

Modelling these types of systems is a matter of deciding the amount of complexity one wants to have. The most complex of course, would be one in which all the constituents of the system are modelled, such as a molecular dynamics type simulation [17]. Of course these types of simulations are computationally prohibitive; they require larger of amounts of both computing power and time in order to be accurate. However, using a field theory to model these systems can be very beneficial in terms of time and simplicity of execution.

2.1.2 Self Consistent Field Theory as Applied to Polymer Systems

Self-consistent field theory (SCFT) is an approximate mean field theory that has seen much success in the study of polymer melt systems. A mean field theory is merely a theory in which the system is assumed to ignore the effect of thermal fluctuations. Using this in conjunction with the fact that the free energy can be written in terms of density fields and chemical potential fields, one can calculate the density morphology that minimizes the free energy. It has been used to study

many different properties such as the excluded volume effect and the order-disorder phase boundary of polymer melt systems [17], and has had great success in doing so.

When simulating these polymer interactions using field theory the interactions between polymers are treated as zeroth order interactions specified by the Flory-Huggins parameter χ . In terms of SCFT simulations the value of the χ parameter determines the strength of the interaction between two different species of polymer, but only if they are in direct contact. Multiple different polymers can be attached at a single end (miktoarm or star) or attached linearly (end to end), and for each polymer there is a χ parameter associated that determine the strength. Since the polymers themselves have length to the individual polymer strands they have spatial extent, and with this extent the interaction also has spatial extent. With this type of interaction they are able to self assemble into a variety of different micro structures, depending on the total amount of unique polymer types in the system and the total volume they occupy.

Work by Matsen and Schick allowed the computation of these equilibrium morphologies of diblock copolymer systems by expanding the spatially dependent fields so that the expansions mimic the symmetry of the phases under consideration. Doing so allowed the study of the stability of the equilibrium of these phases by looking at the free energies of these systems, a lower free energy resulting in a more stable final state. It is easy to see that one can explore the different types of morphologies and compare the free energies to see if one is stable over the other. They also showed and confirmed with experiment that the perforated lamella phase was only meta stable and would eventually become a gyrodial phase after enough time [30, 31]. The drawback of their method is that it requires knowledge of the morphology in question, but allowed the precise calculation of the free energy [29], which can be used to study stability.

Work by Fredrickson *et al.* [17] explored the parameter space of the system in order to search for new phases for copolymer melts. Using this model for an ABC miktoarm system, while keeping the amount of two of the polymer types equal,

Fredrickson found a total of 6 different phases in two dimensions. The different phases found are found in figure 2.3.

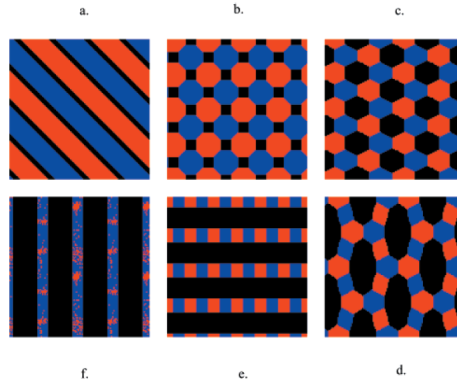


FIGURE 2.3: A plot of the results in [17]. These 6 phases represent the phases found for a triblock copolymer in which $\chi_A = \chi_B = \chi_C$. The volume fractions (f_A, f_B, f_C) are changed accordingly to each run with $f_B = f_C$ and f_A is increased. (a) Lamella (0.2,0.4,0.4) (b) octagon-octagon-tetragon (0.22,0.39,0.39) (c) Honeycomb Hexagon (0.38,0.31,0.31) (d) (0.46,0.27,0.27) (e) (0.54,0.23,0.23) (f) (0.62,0.19,0.19). Taken from [17]

Work by Tang *et al.* [42] improved further the implementation of Fredrickson by differing the amount of different polymers present and how that affected the equilibrium of the system. Tang found that by varying the volume fractions in a deliberate, way a variety of different microphase structures could form. Using SCFT simulations, they have found a total of nine ordered stable phases for ABC triblock star polymers, using symmetric and non-symmetric interaction parameters. Using just symmetric parameters they found a total of seven unique phases represented in figure 2.4.

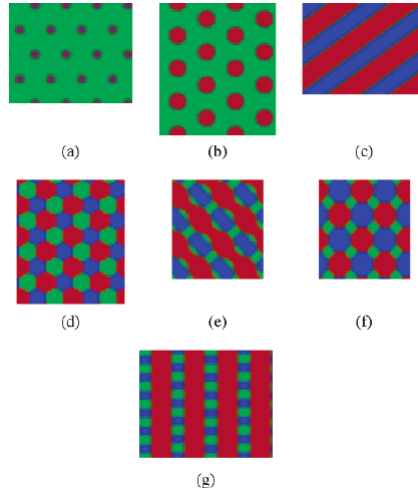


FIGURE 2.4: A schematic of the of the results in [42]. These 7 phases represent the phases found for a triblock polymer in which $\chi_A = \chi_B = \chi_C$. The volume fractions (f_A, f_B, f_C) are changed accordingly to each run, and the sizes of the computational box are adjusted to optimize the free energy. (a) hexagonal lattice phase (0.1,0.8,0.1) (b) core-shell hexagonal phase (0.1,0.7,0.2) (c) three color lamella (0.1,0.5,0.4) (d) three color hexagonal honeycomb phase (0.3,0.4,0.3) (e) knitting pattern (0.1,0.7,0.2)(f) octagon-octagon-tetragon phase (0.2,0.5,0.3) (g) lamella with beads (0.2,0.6,0.2). Taken from [42]

Work by Zhang *et al.* [54] has found that an even more systematic study of the ABC triblock copolymer system resulted in more possible phases. They chose to focus on the phases possible that are based on Archimedean tiling patterns, which are based on tessellation of simple polygons. Some the tiling patterns found by Zhang for ABC star triblock copolymers, represented in figure 2.5, agreed with experiment and other simulations in two dimensions. These studies show the ability for these polymers to self assemble in even more exotic structures. These structures are extremely intricate and some of them have not been not been confirmed with experiment as of yet [54].

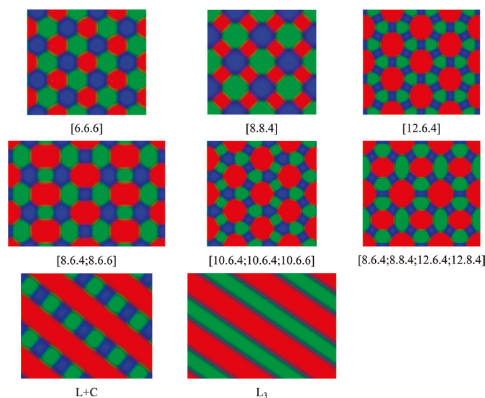


FIGURE 2.5: A schematic of the of the results found in [54]. These 8 phases represent the phases found for a triblock copolymer in which $\chi_A = \chi_B = \chi_C$ for a small section of the parameter space (see figure 4.3). Using notation in which [A,B,C] represents the number of connections each polymer makes with the other polymer types. For example [6,6,6] represents that polymer A is surrounded by 6 independent shapes. For cases in which the shapes are alternating through the overall pattern multiple notations are used. Taken from [54]

Using a set of χ parameters and varying the volume fraction it is possible to explore a variety of different phases. Fredrickson finds a total of 6 different phases, by setting $\chi_{AB} = \chi_{AC} = \chi_{BC}$ and $f_B = f_C$, and varying the final volume fraction [17]. Tang *et al.* [42] examines the same situation, and finds seven possible phases for miktoarm copolymers. Tang's results do not agree with Fredrickson's exactly but they do a more extensive search of the parameter space of volume fractions, and as such they have found 7 different phases for this type of polymer system. The work by Zhang *et al.* does a more specific search of the parameter space, when the global volume fractions are close to being equal. Zhang finds a total of 4 more complicated phases in this region of the parameter space.

Figure 2.3, 2.4 and, 2.5 are morphologies from Fredrickson *et al.* Tang *et al.* and Zhang *et al.* respectively. The honeycomb lattice phase, lamella phase, the lamella with beads phase and the octagon-octagon-tetragon are present in all the results. Tang's results are more specific and broader than the results of Fredrickson. Notice that Zhang has 4 phases that are not found in the results of Tang. These results are chronological in order, and it is expected that more phases could be found, using more specific techniques. Zhang has the most complete of the results, but there is some disagreement between the 3 results. In figure 2.3 the fourth result d)

is a phase that does not appear in the other 2 papers. It is reasonable to assume that the phases that are found to be in common between these three papers are the ones that are the most common and robust phases for a ABC miktoarm system. As such, any model wishing to replicate the results of a miktoarm polymer should be able to recreate these results.

2.2 Colloidal Nano-Particles

A colloid is a system in which a particulate is suspended in some type of solution, like milk or an aerosol. The particles themselves are on the micrometer scale and thus are mainly affected by thermal fluctuations. There are a variety of different methods one can use to cause colloidal particles to self assemble or aggregate in a desired way. One method is to use heterogeneously charged particles to form the aggregates in solution [6]. By giving the particles themselves different charges, the equilibrium state can be altered. The charge on the particles can be altered in this case by changing the pH values in the solvent.

Another method for self-assembling nano-particles is the use of polymer grafted colloids to cause aggregation among the particulates [1]. By varying the amount of polymers grafts onto the colloids, the final equilibrium state can be altered from sheets to aggregate clumps. This provides yet another tool in designing microstructures, with the user controlling the concentration in polymers to affect the ground state of the system. Akcora *et al.* showed that just like polymer systems, colloids, under the right conditions, were able to self assemble.

Polymers grafted onto colloids, DNA can be grafted on to the colloids instead. Due to the unique bonding properties of DNA and the programmable nature of the interactions, they are well suited to be used as the building blocks of a self-assembled material [32]. The pairing is well suited to controlling the aggregation of the colloids due to thermal reversibility of the system as well as the specification of the interactions [49]. By having complementary DNA strands on different colloids the colloidal species will attract to one another through the DNA and aggregate

[32]. Alternatively one can use two competing DNA strands and in the solution a series of “linker” DNA can be used. The upside of linkers is that one can use a single type of DNA strand to mediate the reaction, however as a two step reaction the system is prone to unwanted binding between different linkers [32].

Mirkin *et al.* demonstrated that DNA grafted onto gold nano-particles will form crystalline structures in equilibrium [34, 35]. They also showed that higher temperatures were necessary for the formations of the crystals. Mirkin showed the ability to control the optical properties of the solution material, which is dependent on the particle size, and the inter-particle distance [34]. Near the same time Alivisatos *et al.* used DNA coated gold nano-particles to self-assemble into aggregate clumps that are well defined and soluble [2].

In theory any sort of non-interacting base can be used as the colloid. This gives further control to the different electronic and optical properties a material can have.

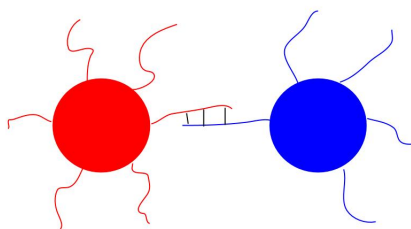


FIGURE 2.6: A simple schematic of a pair of colloids that interact with each other using complementary DNA. The pair have matching nucleotides on the DNA and thus can attach to each other and form a bond. By choosing the DNA correctly one can tailor the interactions between multiple species.

The enthusiasm for using DNA coated colloids (DNACCs) for building materials at the nano-level waned following the work of Mirkin, mostly due to the difficulty in growing engineered structures. One of the main problems is in knowing how to tailor the interactions so that the microstructure that is obtained is the one that is desired. Proper simulation of DNACCs will allow one to explore the different

equilibrium structures and the interactions that result in those structures. Di Michele *et al.* states that the most successful strategy is in using smaller nano-sized colloids, since the decreased interaction strength and the increased mobility of the colloids increase the chances of crystallization [32]. Micrometer colloids with a higher amount of DNA strands attached have the tendency to become kinetically trapped in an unwanted configuration due to the higher number of bondings that can occur. Furthermore, almost no work has been done on using more than two types of colloids or with two colloids that have different densities to design materials [32]. It has been shown that self-assembly using DNA can be achieved in one and two dimensions [24, 27], with the difficulty being in 3 dimensions.

Nykypauchuk *et al.* [19] have developed strategies to build three dimensional nano-structures. They have shown that DNACCs will form crystalline structures at the right temperature. Nykypauchuk also showed that at certain temperatures crystalline structures will form reliably. Even with these successes, using DNACCs is still a relatively new technique that still has a number of hurdles to overcome [32].

2.2.1 Modelling For Self-Assembling DNA Colloids

In order for a system of colloids to self assemble into a certain phase the components have to be interacting with one another in some way. In order to model these systems it is important to look at different ways that this interaction can come about. In terms of the interaction, Martinez-Veracoechea *et al.* [28] has mentioned that the phase of the system cannot be captured by an isotropic pair potential between the colloids. However Tindemans *et al.* [43] have stated that with the use of a two length scale interaction that goes beyond nearest neighbour, this restraint can be circumvented.

Tindemans *et al.* have taken a lattice approach to solving for the equilibrium state for a system of DNA colloids [43]. Using a simple lattice based model to

determine interaction strength, they were able to simulate a system of many interacting particles. The design rules for a system with a number of different particles interacting is of much interest when choosing a model for DNACCs. The Tindemans model is a simple lattice based method in which each lattice site is occupied by a particular particle type (A,B,C, ...). Since the particles are on a lattice the distances are defined by the lattice length constants. Nearest neighbours to a particular particle type will have a certain interaction strength, and the next nearest neighbour will have a different particle interaction. This method can be used to put a restriction on the length scale necessary to design wanted morphologies, since interaction distances are determined entirely by the lattice used. Based on the lattice type, the minimum interaction distance was found to be different; for a triangular lattice the distance was nearest neighbour for example, and for a square lattice the distance was the second nearest neighbour.

Tindemans found that a two length scale interaction can lead a system of interacting particles to form a unique ground state. Nearest neighbor attraction with long range repulsion was found to be a simple recipe to guarantee a unique ground state [43]. A two length scale interaction is an important starting point in deciding how the potential will look in general for systems that are not bound on a lattice.

Archer *et al.* [3, 4] looked at a case of interacting particles in a fluid using mean field density functional theory (DFT). Like Tindemans *et al.* they used a two length scale interaction between the colloids, but they also included a term for the hard sphere interaction. They found phases that shared similarities with the phases found using SCFT for diblock copolymers. They applied their technique only to two dimensional phases.

The field theory based simulations developed by Fredrickson *et al.* were first used to study the different phases for polymer melts. SCFT can also be applied to theoretically similar systems such as DNACCs in a solution, such as what Varilly *et al.* has done [48]. The interaction between two DNACCs was examined using self-consistent field theory. Varilly's goal was to find the potential felt between two DNACCs, and to quantify how this potential scaled with distance. They found

that the interaction strength depended on the amount of DNA that was grafted onto the colloid itself.

The work of Martinez-Veracoechea *et al.* found that the phases possible is highly dependent on the amount of DNA strands on the particles themselves [28]. When the amount of DNA coated on the colloid is too low the ability for the system to crystallize is impossible. They found that with more strands the colloid was able to form bonds with more colloids around it. This means that with more strands a more mechanically stable material is more easily obtained.

Chapter 3

Theory

3.1 Phase Separation

When two species mix together and do not form a homogeneous mixture they will macrophase separate from one another. For example when oil and water are mixed together two distinct regions will form, one with just water and one with just oil. The interactions between oil and water force the system to favour a system in which the two species are distinct.

In a copolymer mix, the different blocks can be incompatible to one another and will have a tendency to unmix and form two distinct regions in the solution. However, the polymer blocks are bonded to one another so they can only separate so far from each other. The same basic process can happen in DNA coated colloids [32] with the colloids attracting to each other through DNA strands. This is called microphase separation and it is important to the forming of nano scale microstructures. The forming of these structures is dependent on the system finding a balance between increasing its entropy and minimizing the energy between the different components.

3.2 N Particles with Isotropic Interactions

A simple model has been developed between two particles that interact under an isotropic potential, a potential that is uniform in all orientations [23]. This model can be easily expanded to a N particle system with n_s particles of species s , where N different particle species interact with N different potentials. We want to expand this type of system into the language of SCFT so as to analyse the effect of more species on the equilibrium morphologies.

3.2.1 Hamiltonian

The Hamiltonian for a system of n_s particles of species s , that interact under some potential will take the form of:

$$H = \sum_{i=1}^{n_s} \frac{p_i^2}{2m} + \frac{1}{2} \sum_{i=1}^{n_s} \sum_{j=1}^{n_s} U(|\mathbf{r}_i - \mathbf{r}'_j|). \quad (3.1)$$

The potential $U(|\mathbf{r}_i - \mathbf{r}_j|)$ represents interactions between particles, and the term $i = j$ represents self interactions. Let us note that these self interaction terms will add up to a constant and do not affect the free energy and can be ignored.

It is useful to define the idea of a density function to describe the spatial densities of the particles. For a species s :

$$\hat{\phi}_s(\mathbf{r}) = v_s \sum_{i=1}^{n_s} \delta(\mathbf{r} - \mathbf{r}_{i,s}) \quad (3.2)$$

where v_s is the volume that particle s occupies and $\mathbf{r}_{i,s}$ represents the position of a particle of species s . The particle at position $\mathbf{r}_{i,s}$ is localized entirely at that point,

the delta function acts as the mechanism in which this localized particle is spread about some volume v_s . Integrating both sides of this equation over the volume size we get:

$$\int d\mathbf{r} \hat{\phi}_s(\mathbf{r}) = v_s \int d\mathbf{r} \sum_{i=1}^{n_s} \delta(\mathbf{r} - \mathbf{r}') = n_s v_s = f_s V \quad (3.3)$$

where f_s is the volume fraction of species s and V is volume of the system in question. This is a smoothed out version of the density function equation 3.2. Here we defined the volume fraction as:

$$f_s = n_s \frac{v_s}{V} \quad (3.4)$$

which can be thought of as the amount of volume that a species s will occupy in the total volume. Since the system can be described as incompressible, which means the total density in the volume V is constant. It necessarily follows that the sum of all the volume fractions has to equal one.

We can also define the particle size measure:

$$\frac{v_s}{v_0} = \alpha_s \quad (3.5)$$

where v_0 is some reference volume which can be chosen for convenience.

We will also need the potential written in terms of the density function. For a system of N different species there will be a certain number of pair potentials that can be described. For example if we have two particles (A, B) we can have three different potentials U_{AA}, U_{AB}, U_{BB} . In general the number of pair wise potentials that can be given with N species is:

$$\frac{N!}{(N-2)!2!} + N. \quad (3.6)$$

The first term in 3.6 accounts for the different pairings between particles and the second term is for pairing between like particles. With this in mind we can write the total potential of the system as a sum of these individual pair wise potentials.

$$U(\{\mathbf{r}_A\}, \{\mathbf{r}_B\}, \dots) = \sum_{s=1}^N \left(\sum_{i=1}^{n_s} \sum_{j<i}^{n_s} U_{ss}(|\mathbf{r}_i - \mathbf{r}_j|) \right) + \sum_{s=1}^N \sum_{s'>s}^N \left(\sum_{i=1}^{n_s} \sum_{j=1}^{n_{s'}} U_{ss'}(|\mathbf{r}_i - \mathbf{r}_j|) \right). \quad (3.7)$$

The first term represents the potentials of a species s interacting with itself (U_{AA}, U_{BB}, \dots), the second term represents the interactions between species of different types. Using equation 3.2 we can write the potential in terms of the density functions by integrating over the two spatial positions for n_s different species:

$$U(\hat{\phi}_A(\mathbf{r}), \hat{\phi}_B(\mathbf{r}), \dots) = \int \int d\mathbf{r} d\mathbf{r}' \left[\sum_{s=1}^N \frac{1}{2v_s^2} \hat{\phi}_s(\mathbf{r}) U_{ss}(|\mathbf{r} - \mathbf{r}'|) \hat{\phi}_s(\mathbf{r}') \right. \quad (3.8) \\ \left. + \sum_{s=1}^N \sum_{s'>s}^N \frac{1}{v_s v_{s'}} \hat{\phi}_s(\mathbf{r}) U_{ss'}(|\mathbf{r} - \mathbf{r}'|) \hat{\phi}_{s'}(\mathbf{r}') \right].$$

Instead of dealing with the specific positions of all the different particles, we have a potential that only deals with the densities of particles at any particular point. This lets us phrase the overall potential in terms of different species, and now the individual particle positions no longer need to be tracked.

Now we can assume that the system is incompressible, which can be placed into the equations as the constraint:

$$1 = \sum_{i=1}^N \hat{\phi}_i(\mathbf{r}). \quad (3.9)$$

With this constraint we can eliminate terms in potential, by rephrasing it in terms of effective interactions between different species. The constraint can be applied to the potential 3.8 and then terms with the same density products can be collected in the form of:

$$\hat{\phi}_s \left(\frac{1}{2} U_{ss} - U_{ss'} + \frac{1}{2} U_{s's'} \right) \hat{\phi}_{s'}. \quad (3.10)$$

$s \neq s'$

If we can call the new potential term $U_{ss'}$ which is the effective interaction between two particles of different species s and s'

$$U(\hat{\phi}_A(\mathbf{r}), \hat{\phi}_B(\mathbf{r}), \dots) = \int \int d\mathbf{r} d\mathbf{r}' \times \quad (3.11)$$

$$\sum_{s=1}^N \sum_{s' > s}^N \frac{1}{v_s v_{s'}} \hat{\phi}_s(\mathbf{r}) U_{ss'}(|\mathbf{r} - \mathbf{r}'|) \hat{\phi}_{s'}(\mathbf{r}')$$

This describes the total potential now in terms of the density function and the effective potential.

3.2.2 Partition Function

Now we can calculate the partition function for this type of system. The classical canonical partition function for a system of n_s interacting particles of species s :

$$\begin{aligned}
 Z &= \prod_{s=1}^N \frac{1}{n_s! h^{3n}} \int \int d\mathbf{r}^{n_s} d\mathbf{p}^{n_s} e^{-\beta H(\mathbf{r}, \mathbf{p})} \quad (3.12) \\
 Z &= \prod_{s=1}^N \frac{1}{n_s! h^{3n}} \int \int d\mathbf{r}^{n_s} d\mathbf{p}^{n_s} e^{-\beta(\sum_{i=1}^{n_s} \frac{p_i^2}{2m} + \sigma^6 \int \int \frac{d\mathbf{r}}{\sigma^3} \frac{d\mathbf{r}'}{\sigma^3} \sum_{s' > s}^N \frac{1}{v_s v_{s'}} \hat{\phi}_s(\mathbf{r}) U_{ss'}(|\mathbf{r}-\mathbf{r}'|) \hat{\phi}_{s'}(\mathbf{r}))}
 \end{aligned}$$

where an arbitrary length scale σ is introduced to make the argument of the integral dimensionless and $n = \sum_{s=1}^N n_s$. We have written here the total partition function, which the reader can note is just the product of the individual partition functions for each species s . The h term is Planck's constant and accounts for the discrete nature of the phase space when integrating. Integrating over the momentum in the partition function we get:

$$Z = \prod_{s=1}^N \frac{1}{n_s! h^{3n} \lambda_{T,s}^{3n_s}} \int d\mathbf{r}^{n_s} e^{-\beta(\int \int \frac{d\mathbf{r}}{\sigma^3} \frac{d\mathbf{r}'}{\sigma^3} \sum_{s' > s}^N \frac{\sigma^6}{v_s v_{s'}} \hat{\phi}_s(\mathbf{r}) U_{ss'}(|\mathbf{r}-\mathbf{r}'|) \hat{\phi}_{s'}(\mathbf{r}))} \quad (3.13)$$

where λ_T is equal to [38]

$$\lambda_T = \left(\frac{2\hbar^2}{mk_b T} \right)^{\frac{1}{2}}. \quad (3.14)$$

This term is known as the classical thermal de Broglie wavelength, where T is the temperature in Kelvin, the k_b is Boltzmann's constant, m is the mass of the particle, and \hbar is the reduced Planck's constant.

Now we transform the partition function into a functional integral, using the known identity [17]:

$$\int \mathcal{D}\phi \delta(\phi - \hat{\phi}) = 1. \quad (3.15)$$

Equation 3.15 is a functional integral, which is an integral where the domain is no longer a set of numbers, but over a space of functions. Just like in the regular integral case, the integral over a Dirac delta function will equal 1. This identity can be used to rewrite the partition function as a functional integral over the density functions representing the particles.

$$Z = \prod_{s=1}^N \frac{1}{n_s! h^{3n} \lambda_{T,s}^{3n_s}} \int d\mathbf{r}^{n_s} \int \mathcal{D}\phi_s \delta(\phi_s - \hat{\phi}_s) \times \quad (3.16)$$

$$e^{-\beta \left(\int \frac{d\mathbf{r}}{\sigma^3} \frac{d\mathbf{r}'}{\sigma^3} \sum_{s' > s}^N \frac{\sigma^6}{v_s v_{s'}} \phi_s(\mathbf{r}) U_{ss'}(|\mathbf{r} - \mathbf{r}'|) \phi_{s'}(\mathbf{r}) \right)}.$$

We then follow the same procedure as illustrated in [17] and express the delta functional as an integral over a set of real fields. The Dirac delta function can be defined as an integral over a set of Fourier variables. As such the single variable form takes the form of:

$$\delta(x - \hat{x}) = \int_{-i\infty}^{i\infty} dk e^{k(x - \hat{x})}. \quad (3.17)$$

where x and k are conjugate Fourier variables. For the functional representation we replace the regular real variable with functions that represent the density and chemical potential fields and the integral is now a functional integral over W .

$$\delta(\phi - \hat{\phi}) = \int_{-i\infty}^{i\infty} \mathcal{D}W e^{\int \frac{d\mathbf{r}}{v_0} W(\mathbf{r})(\phi - \hat{\phi})}. \quad (3.18)$$

Using this identity in the partition function it is important to note that you get a series of products for each different species of particles in the system.

We can take definition 3.16 and write the partition function as a functional integral over the real density fields ϕ and the chemical potential fields W_s .

$$Z = \prod_{s=1}^N \frac{1}{n_s! h^{3n} \lambda_{T,s}^{3n_s}} \int \int \mathcal{D}\phi_s \mathcal{D}W_s Q_s^{\frac{f_s V}{v_s}} \times \quad (3.19)$$

$$e^{-\beta \left(\int \frac{d\mathbf{r}}{\sigma^3} \frac{d\mathbf{r}'}{\sigma^3} \sum_{s < s'}^N \frac{\sigma^6}{v_s v_{s'}} \phi_s(\mathbf{r}) U_{ss'}(|\mathbf{r} - \mathbf{r}'|) \phi_{s'}(\mathbf{r}') + \int \frac{d\mathbf{r}}{v_0} \phi_s(\mathbf{r}) W_s(\mathbf{r}) \right)}.$$

We can now define the weighting term for the partition function for a single particle of species s as Q_s

$$Q_s = \int \frac{d\mathbf{r}}{v_0} e^{-\frac{v_s}{v_0} \omega_s(\mathbf{r})}. \quad (3.20)$$

We can now apply the saddle function approximation onto this functional integral. This approximation is used to determine the value of integrals by setting the value of the integral equal to the maximum value of the integral (which will minimize the free energy).

We look to the discussion by Das [5] to motivate the use of the saddle function approximation in this context. We are looking to approximate a functional integral in the form:

$$U = \int \mathcal{D}x e^{S[x]}. \quad (3.21)$$

There exists a path that will satisfy:

$$\left. \frac{\delta S[x]}{\delta x} \right|_{x=x_c} = 0 \quad (3.22)$$

where x_c represents the minimum of the functional $S[x]$. We can expand the functional $S[x]$ by defining $x(t) \equiv x_c(t) + \eta(t)$ and expanding around the minimum of the functional.

$$S[x] = S[x_c] + \frac{1}{2} \int \int dt_1 dt_2 \eta(t_1) \frac{\delta^2 S[x_c]}{\delta x_c(t_1) \delta x_c(t_2)} \eta(t_2) + \dots \quad (3.23)$$

We can use this expansion in equation 3.21 to calculate the value of the integral. By assuming the higher order terms in the expansion are small and only keeping the lowest term we see that equation 3.21 becomes:

$$U \approx \mathcal{N} e^{S[x_c]} \quad (3.24)$$

where we have \mathcal{N} is a constant of normalization.

In this case we are looking for the set of fields that minimize the action of the Hamiltonian. This strategy is the basis of performing a mean field approximation for a system. Fluctuations around the equilibrium point are assumed to be small and negligible, which is the basis for allowing the argument of the exponential to be replaced by the value it takes near equilibrium. Quantitatively we have the conditions:

$$\left. \frac{\delta H[\phi(\mathbf{r}), W(\mathbf{r})]}{\delta \phi(\mathbf{r})} \right|_{\phi(\mathbf{r})=\phi(\mathbf{r})'} = 0 \quad (3.25)$$

$$\left. \frac{\delta H[\phi(\mathbf{r}), W(\mathbf{r})]}{\delta W(\mathbf{r})} \right|_{W(\mathbf{r})=\omega(\mathbf{r})'} = 0 \quad (3.26)$$

Theory.

where $\phi(\mathbf{r})', \omega(\mathbf{r})'$ represent the fields that minimize the action of the Hamiltonian. These two primed variables represent the conditions for equilibrium. With this we can approximate the partition further by:

$$Z \approx \prod_{s=1}^N \frac{1}{n_s! h^{3n} \lambda_{T,s}^{3n_s}} Q_s^{\frac{f_s V}{v_s}} \times e^{-\beta \left(\int \frac{d\mathbf{r}}{\sigma^3} \frac{d\mathbf{r}'}{\sigma^3} \sum_{s < s'}^N \frac{\sigma^6}{v_s v_{s'}} \phi_s(\mathbf{r}) U_{ss'}(|\mathbf{r} - \mathbf{r}'|) \phi_{s'}(\mathbf{r}') + \int \frac{d\mathbf{r}}{v_0} \phi_s(\mathbf{r}) \omega_s(\mathbf{r}) \right)} \quad (3.27)$$

In using the saddle function approximation we have ignored the normalization constant \mathcal{N} , overall it will just add a constant to the free energy and thus can be ignored.

The prime on ϕ, ω was dropped for convenience. With this we can calculate the approximate Helmholtz free energy functional using $F = -k_b T \log(Z)$, where log is the natural logarithm.

$$\begin{aligned} \frac{v_0 F}{k_b T V} = & - \sum_{i=1}^N \log \left(\frac{1}{n_i! h^{3n} \lambda_{s,T}^{3n}} \right) - \frac{f_i}{\alpha_i} \log \left(\frac{v_0 Q_i}{V} \right) + \frac{v_0}{V} \int \frac{d\mathbf{r}}{v_0} \left\{ \int \frac{d\mathbf{r}'}{v_0} \frac{1}{2} \times \right. \\ & \sum_{i=1}^N \sum_{j=1}^N [\phi_i(\mathbf{r}) - f_i] \frac{U_{ij}(|\mathbf{r} - \mathbf{r}'|)}{\alpha_i \alpha_j k_b T} [\phi_j(\mathbf{r}') - f_j] \\ & \left. - \sum_{i=1}^N w_i(\mathbf{r}) \phi_i(\mathbf{r}) + \frac{\kappa}{2} \left(\sum_{i=1}^N \phi_i(\mathbf{r}) - 1 \right)^2 \right\} \end{aligned} \quad (3.28)$$

where we have scaled the free energy by average kinetic energy $k_b T$ and $\frac{v_0}{V}$ to create the free energy density, and we have added a term not originally present in the Hamiltonian. The volume fractions have been subtracted to readjust the zero of the free energy. The final term is the incompressibility term which adds an energy penalty to the system for violating incompressibility, with a numerical term κ chosen high enough to ensure that globally the excluded volume is conserved. This technique was developed by Eugene Helfand to ensure global conservation of

the incompressibility and this technique has been used numerous times in polymer models that use SCFT [16, 21]. In principle the incompressibility energy penalty could have been included as a term in the Hamiltonian and carried through the derivation. Since our particles have no particular structure a mechanism is needed to keep the ensemble averaged excluded volume in place. It is easier to place this incompressibility mechanism into the free energy as we wish to have the global excluded volume effect to be obeyed. It allows us to design a system with no fixed size for the particle, so that a hard sphere interaction does not need to be included in order to maintain structure. The incompressibility will mimic the hard sphere interaction very close to the center of the particle, but does allow some flexibility in the radius of the particles themselves. The constant total volume of the mixture gives the ensemble average excluded volume, but since at the particle level the excluded volume is not enforced, the packing structure of the system is lost [46].

In order to find the equilibrium density of this system we take the functional derivative of the free energy with respect to the density and the chemical potential and set both equal to zero. Doing so yields a system of coupled and non linear equations representing the density and chemical potential fields for all the different species in the system.

$$\phi_i(\mathbf{r}) = \frac{f_i V}{v_0 Q_i} e^{-\alpha_i \omega_i(\mathbf{r})} \quad (3.29)$$

$$\omega_i(\mathbf{r}) = \int \frac{d\mathbf{r}'}{v_0} \sum_{j=1}^N \phi_j(\mathbf{r}') \frac{U_{ij}(|\mathbf{r} - \mathbf{r}'|)}{\alpha_i \alpha_j k_b T} + \kappa \left(\sum_{k=1}^N \phi_k(\mathbf{r}) - 1 \right) \quad (3.30)$$

where:

$$Q_i = \int \frac{d\mathbf{r}}{v_0} e^{-\alpha_i \omega_i(\mathbf{r})}. \quad (3.31)$$

These equations represent the equilibrium conditions of the system. There is a set of two equations for each of the different types of particles in the the system.

The $\phi_s(\mathbf{r})$ terms are similar in nature to the Boltzmann distribution, a probability distribution that is weighted by the energy. $\phi(\mathbf{r})$ represents the volume fraction of a particular species at a point \mathbf{r} , which is weighted by a term that looks similar to a regular Boltzmann weight. The $\omega_s(\mathbf{r})$ represent something akin to a chemical potential field, the function itself describes the “energy landscape”. The energy landscape describes the regions where there are energy penalties and advantages based on where the other particles in the system are. This landscape is of course dependent on the particle-particle interaction, and the incompressibility which puts a limit on the particle density at a given point. It is easy to see that both of these conditions are dependent on each other and this is the reason as to why this is called self consistent field theory, as the solution needs to be self consistent.

3.2.3 Potential

So far the potential U_{ij} has been undefined, only representing some form of interaction between two species. The potential is really the central point of the problem as it is how we can control the phase of the system. We wish to restrict ourselves to isotropic pair potentials as the interaction scheme of choice. Martinez-Veracoechea *et al.* [18] states that no self-assembly can take place between two interacting particle under a purely isotropic interaction. Frenkel *et al.* explains that the work of Tindemans [43] indicates that as long as the isotropic potential does not interact only with nearest neighbours, the concerns of Martinez-Veracoechea are not merited. Thus, unlike basic polymer models, we need an interaction that is spatially expansive. Tindemans *et al.* [43] state that in order to have non-trivial morphologies develop the particles have to interact on 2 different length scales not counting any excluded volume interaction. Tindemans uses a latticed based approach and thus the potential is defined by the lattice constant. The interaction is broken up into attractive nearest neighbour interactions and repulsive next nearest neighbour

interactions. Thus we look to implement a potential that is non-local and has two different interaction regions.

Buldyrev *et al.* and Hoye *et al.* used a potential that has a hard core, and a soft repulsion as the potential for their systems [9, 22]. The hard core of the potential defines the size of the particle, while the soft repulsions define the interactions between the particles themselves. Wang *et al.* used soft core potentials to allow for particle “overlapping” or a non fixed radius for the particles, which is well suited to studying the equilibrium properties of soft matter systems [51].

Since we are mainly interested in looking at soft matter systems we choose not to use a hard core potential. Since we have an energy penalty in the free energy to avoid too much overlapping of the particles, we do not need a hard core potential to maintain structure.

We also restrict the potential to be everywhere continuous and the derivative must also be continuous in that range. This feature is necessary since, when using a Fast Fourier Transform (FFT) based algorithm, the potential itself will need to be discretized, and any singularities in the potential will change the behaviour of the potential near the singularity depending on the discretization [23]. This means a standard potential, such as Lennard-Jones, will not meet these requirements since it diverges at the origin, and is not a two length scale potential excluding the core repulsion.

Using the potential that is prescribed in reference [23], we make a slight modification to the potential by reversing the attractive and repulsive sections in order to account for the fact that our potentials describe the interaction between different species and the original potential describes like species interactions:

$$\frac{U_{ij}}{k_b T} = \begin{cases} \frac{A_1 + A_2}{2} \cos\left(\frac{\pi r}{\lambda}\right) + \frac{(A_1 - A_2)}{2}, & r \leq \lambda \\ -A_2 \exp\left[\frac{-(r - \lambda)^2}{2\gamma^2}\right], & \text{otherwise} \end{cases} \quad i \neq j \quad (3.32)$$

where:

- A_1 is the max height of the repulsive part of the potential
- A_2 is the max depth of the attractive part of the potential
- λ is the length to the minimum of the potential
- γ is the standard deviation of the attractive Gaussian of the potential

A_1, A_2 are dimensionless, and scale inversely with the temperature of the system. As such setting $A_1 = A_2 = 0$ is equivalent to looking at the infinite temperature case. Conversely $A_1 = A_2 = \infty$ is equivalent to looking at a system that is at absolute zero. λ controls the length scales of the potential, how far the repulsive part extends and γ controls the width of the long range attraction, respectively. One of the length scales in the potential can be normalized out, by setting it equal to one, and having all the other lengths in the model be in terms of one of the potential length scales.

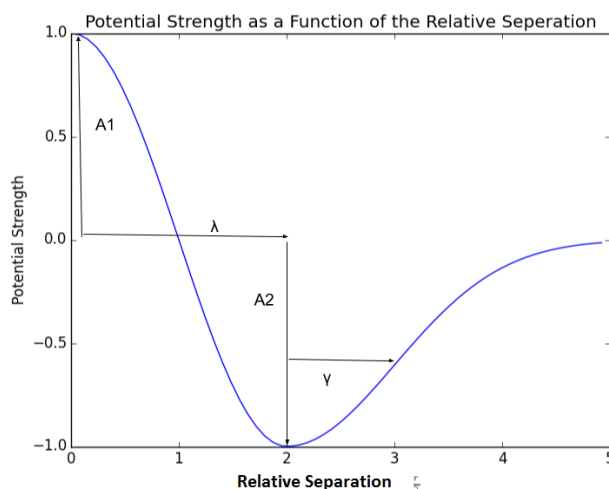


FIGURE 3.1: A plot of the potential used in this model. The x-axis represents the separation scaled by the chosen standard lengths scale. The y-axis represents the scaled strength of the potential.

3.2.4 Computation of SCFT equations

The self consistent equations 3.29 are both coupled and non linear. We have several different parameters that can be adjusted in the computation of this system which

can increase the difficulty of finding a solution. A numerical method is needed that is both stable and numerically efficient.

It is possible to use the spectral methods pioneered by Matsen and Schick, by expanding the field functions in a Fourier basis. These methods, however, require some pre-existing knowledge of the symmetries of the system [29]. This is a drawback when one is considering using this type of particle based model to explore a variety of different equilibrium solutions for different potential parameters. We instead will use the same method as von Konigslow *et al.*, and do an iterative approach over the densities.

To lower the number of computational variables we choose the potentials for the different particle interactions to be the same. This means that all particles interact with every other type of particle using the same potential parameters, thus only one set of potential parameters have to be passed at the beginning of the run. In order to differentiate the particles from one another we use the volume fractions to break the natural symmetries of the system.

It is convenient to specify the standard length scale in this problem to be γ , the standard deviation of the attractive Gaussian part of the potential. This choice fixes γ to be unity further reducing the amount of parameters, as each of the length scales are now measured in units of γ . Choosing either of the two length scales is sufficient to lowering the overall number of variables.

3.2.4.1 Computational Approach

The basic iterative approach for solving equations 3.29 takes the form:

$$\phi(\mathbf{r})^{n+1} = (1 - \rho)\phi(\mathbf{r})^n + \rho\phi(\mathbf{r})^{n+1/2} \quad (3.33)$$

where n is the current step and $n + \frac{1}{2}$ is the step just calculated by inputting ϕ_n into the SCFT equations, and ρ is a mixing parameter. This kind of mixing increases stability, with respect to direct substitution, but can cause the system to spend

a long time converging especially if ρ is chosen to be small. In order to speed up convergence of the system the κ term in the chemical potential equation 3.29 can be varied along with the mixing parameter. Having a large incompressibility creates a larger energy penalty for incompressibility violations but may cause the system to diverge if it is too high, and the mixing parameter is too low. This is countered by making the mixing parameter decrease as the incompressibility increases, which we call a variable incompressibility method.

The two most important parameters for stability are the mixing parameter and the incompressibility. Raising κ has the effect of causing small differences between the densities and unity to have a much larger energy penalty. Making κ larger means that the step size needs to be smaller in order to resolve the densities correctly. A common problem is that when the step size is too small, the system will not converge in a realistic number of steps. κ needs to be large enough so that these differences are minimized, but not so large that the system can't converge at that number of steps. This is the reason a variable step size method is used. κ is limited to 1000 at its maximum and the inverse of it is used as the lowest possible step size needed.

3.2.4.2 Fourier Transforms and Convolutions

The most difficult computational part of the equations are the integrals over the potentials and the density fields, in the chemical potential equation 3.29. It is important to note that integrals in the form:

$$h(x) = \int dx' f(x')g(x - x') \quad (3.34)$$

are called convolution integrals, as they produce a third function that is the area overlap of the original two functions. The equations that govern the chemical potentials contain these convolutions. There is a famous theorem called the convolution theorem which states:

$$\mathcal{F}\{f \star g\} = K * \mathcal{F}\{f\}\mathcal{F}\{g\} \quad (3.35)$$

which means that the Fourier transform (denoted by \mathcal{F}) of the convolution between two functions is equal to the Fourier transform of each individual function multiplied together, along with some normalization constant K . It is easy to see the power of such a theorem here, if we can Fourier transform the two individual functions, multiply them together and then inverse Fourier transform the result. This process will get us the final result of the convolution integral, without having to explicitly perform the integration. We can do this by applying periodic boundary conditions to the system as a whole so that we can Fourier transform the densities, and the potential.

Normally doing this type of computation would not be faster than explicitly computing the convolution integral and applying the boundary conditions. However, in 1965 Cooley and Tukey published a more efficient form of a Discrete Fast Fourier Transform (FFT) that allowed for quick computation of Fourier transforms and thus quick computation of convolutions. Before this, simple application of the definition of the Discrete Fourier Transform would result in a complexity of $\mathcal{O}(n^2)$, with this new algorithm the complexity decreased to $\mathcal{O}(n \ln(n))$ where n is the size of the system [13].

If we apply periodic boundary conditions to our problem we can leverage this theorem for quicker computation of the chemical potential fields.

3.2.4.3 Computation Parameters

The box size was fixed to $L = 10$ in units of γ , which was deemed large enough that a periodic phase would present itself without finite size effects. In theory the length and the width can be adjusted to get rid of any distortions present in the final phase.

It was decided that the the vector norm will be used as our measure for knowing when to stop the program which in this case takes the form:

$$\frac{\int \frac{dr}{v_r} \left(\phi_i^{n+\frac{1}{2}}(\mathbf{r}) - \phi_i^n(\mathbf{r}) \right)^2}{\int \frac{dr}{v_r} (\phi^n(\mathbf{r}))^2} \quad (3.36)$$

where i in this case is just a chosen density. The algorithm finishes once $\phi_i^{n+1} - \phi_i^n \leq \tau$ or $n = n_{max}$, where τ is some tolerance (that is sufficiently small) or the maximum number of iterations have passed. If τ is chosen to be too high then there is a chance that the solution found will be one that is not the true solution to 3.29. $\tau = 10^{-7}$ was chosen to be the limit for most of the runs and is sufficiently small enough to avoid most of these problems.

3.2.4.4 Algorithm

We start the system at some random distribution centred around each of the specimen's volume fraction. Calling this density ϕ_i^0 , we plug it into equation 3.29 and using the predetermined potential we calculate the corresponding chemical potentials ω_i^0 , where i represents the different species. With this new chemical potential we can calculate $\phi_i^{\frac{1}{2}}$ and use equation 3.33 to calculate ϕ_i^1 . These new densities can be used to calculate new chemical potentials, and the iteration can continue to calculate ϕ_i^n, ω_i^n where n represents the current iterative step.

We choose one of the densities to be used to measure convergence. Using equation 3.36 we can see if the new density and the old density are roughly the same within the chosen tolerance. If so, then the solution has been found. However if the maximum number of iterations has been reached we use the variable incompressibility method to attempt to reach a convergent solution. We attempt to raise κ three times and if the solution is still not found during that time then the program is terminated.

3.3 Two Species of Particles with Large Particle Disparity

The particle size measure α has a larger effect on the stability of solving equations 3.29. The current set of equations cannot resolve particle disparity of greater than 100 [23]. It is necessary to rewrite the equations in a more tractable form when looking to analyse systems with large particle disparity.

3.3.1 Issues with SCFT and Particle Size

These two equations:

$$\phi_i(\mathbf{r}) = \frac{f_i V}{v_0 Q_i} e^{-\alpha_i \omega_i(\mathbf{r})} \quad (3.37)$$

$$\omega_i(\mathbf{r}) = \int \frac{d\mathbf{r}'}{v_0} \sum_{j=1, j \neq i}^N \phi_j(\mathbf{r}') \frac{U_{ij}(|\mathbf{r}' - \mathbf{r}|)}{\alpha_i \alpha_j k_b T} + \kappa \left(\sum_{i=1}^N \phi_i(\mathbf{r}) - 1 \right) \quad (3.38)$$

represent the equilibrium volume fractions and chemical potential fields of a system of N particles which interact with one another with some potential U_{ij} where i and j represent the the respective particles and no species interacts with itself. Where Q_i is the single particle partition function:

$$Q_i = \int \frac{d\mathbf{r}}{v_0} e^{\alpha_i \omega_i(\mathbf{r})}. \quad (3.39)$$

Now we can examine what happens to 3.37 and 3.39 when the α parameter becomes very small for one of the particles. It is easy to see that when α_i is taken to the limit $\alpha \rightarrow \infty$, the arguments in the exponential become very large and these equations cannot be resolved numerically on a computer.

For the system in question, looking at equations 3.39 it can be seen that since no matter the argument of the exponential the result will always be positive. This means that the integral over the exponential will also result in a positive number, forcing the $\phi(\mathbf{r})$ term to always be between zero and one. This is a helpful feature in standard SCFT since the volume fractions are naturally normalized. However, when adjusting one of the α_i 's to be small we get results which are not tractable numerically. One of the exponentials will blow up and the results are not resolvable on any computer, meaning the iterative approach outlined before will fail. Using arbitrary floating point implementations are not an option since this will increase the amount of time needed to solve these equations numerically. We would like to be able to use floating point arithmetic and explore systems in which α_i can range as low as 10^{-6} as this is the typical size disparity between nanometer colloid and solution, and with this in mind we need to rewrite the equations.

3.3.2 Derivation of a New Fixed Point Equation

Starting with the free energy (equation 3.28) we can exactly remove the chemical potential fields $\omega(\mathbf{r})$ through substitution and get:

$$\begin{aligned} \frac{Fv_0}{k_bTV} &= \frac{v_0}{V} \int d\mathbf{r} \left\{ \frac{\phi_i(\mathbf{r})}{\alpha_i} \left[\log \left(\frac{\phi_i(\mathbf{r})}{f_i} \right) - 1 \right] \right. \\ &+ \frac{1}{2} \int \frac{d\mathbf{r}'}{v_0} \sum_{i=0}^N \sum_{j=0, j \neq i}^N [\phi_i(\mathbf{r}) - f_i] \frac{U_{ij}(|\mathbf{r}' - \mathbf{r}|)}{\alpha_i \alpha_j k_b T} [\phi_j(\mathbf{r}') - f_j] \\ &\left. + \frac{\kappa}{2} \left(\sum_{i=0}^N \phi_i(\mathbf{r}) - 1 \right)^2 \right\}. \end{aligned} \quad (3.40)$$

The free energy is now written in terms of the densities only.

At this point we will assume that there are only two types of particles in the system, a much larger particle (A), and a particle that is much smaller (B). This is to mimic the situation of a particle inside some solution. We can further modify

the free energy equations to enforce strict incompressibility with equation $\phi_A(\mathbf{r}) + \phi_B(\mathbf{r}) = 1$. In doing so we can rewrite the free energy in terms of one density field $\phi_A(\mathbf{r}) = \phi(\mathbf{r})$:

$$\begin{aligned}
\frac{Fv_0}{k_bTV} &= \frac{1}{V} \int d\mathbf{r} \frac{\phi(\mathbf{r})}{\alpha_A} \left[\log \left(\frac{\phi(\mathbf{r})}{f_A} \right) - 1 \right] \\
&+ \frac{1}{V} \int d\mathbf{r} \frac{1 - \phi(\mathbf{r})}{\alpha_B} \left[\log \left(\frac{1 - \phi(\mathbf{r})}{f_B} \right) - 1 \right] \\
&- \frac{1}{Vv_0} \int d\mathbf{r}' \int d\mathbf{r} [\phi(\mathbf{r}) - f_B] \frac{U_{ij}(|\mathbf{r}' - \mathbf{r}|)}{\alpha_A \alpha_B k_b T} [\phi(\mathbf{r}') - f_A] \\
&+ \frac{\kappa}{2} \left[f_A - \frac{1}{V} \int d\mathbf{r} \phi(\mathbf{r}) \right]^2
\end{aligned} \tag{3.41}$$

where we adjusted the zero of the free energy in order to remove the volume fractions from within the convolution term. Since the zero of the free energy is arbitrary, this does not change the physics of the system but only turns it into a more convenient form.

The use of the strict incompressibility makes this equation weaker as the volume fraction is no longer globally conserved. The final term in 3.41 forces global conservation of the volume fraction, which corrects this problem by adding an energy penalty to the free energy. Notice the first terms in the free energy have the form of the translational entropy found in standard density functional theory (DFT) [3, 4, 46]. Thus we have rewritten the problem in a form that more closely resembles DFT. However unlike DFT we do not have an implicit solvent in our equations.

Using this new free energy we can take the derivative with respect to $\phi(\mathbf{r})$ and find an expression for the minimization of the free energy. By varying 3.41 and setting it equal to zero we get:

$$\begin{aligned}
0 &= \frac{1}{\alpha_A} \log\left(\frac{\phi(\mathbf{r})}{f_A}\right) - \frac{1}{\alpha_B} \log\left(\frac{1 - \phi(\mathbf{r})}{f_B}\right) \\
&\quad - 2 \int \frac{d\mathbf{r}'}{v_0} [\phi(\mathbf{r}') - f_A] \frac{U_{ij}(|\mathbf{r}' - \mathbf{r}|)}{\alpha_A \alpha_B k_b T} - \kappa \left[f_A - \frac{1}{V} \int d\mathbf{r} \phi(\mathbf{r}) \right].
\end{aligned} \tag{3.42}$$

This can be framed in terms of a fixed point equation by adding or subtracting $\phi(\mathbf{r})$ to both sides of 3.42.

$$\begin{aligned}
\phi(\mathbf{r}) &= \phi(\mathbf{r}) - \frac{1}{\alpha_A} \log\left(\frac{\phi(\mathbf{r})}{f_A}\right) - \frac{1}{\alpha_B} \log\left(\frac{1 - \phi(\mathbf{r})}{f_B}\right) \\
&\quad + 2 \int \frac{d\mathbf{r}'}{v_0} [\phi(\mathbf{r}') - f_A] \frac{U_{ij}(|\mathbf{r}' - \mathbf{r}|)}{\alpha_A \alpha_B k_b T} - \kappa \left[f_A - \frac{1}{V} \int d\mathbf{r} \phi(\mathbf{r}) \right]
\end{aligned} \tag{3.43}$$

where $\phi(\mathbf{r})$ has been subtracted from both sides to avoid divergence from a physically meaningful solution.

3.3.3 Computation

3.3.3.1 Fixed Point Equations

Fixed point equations are often found in science and engineering stability problems, and have obvious similarities to root finding problems. A regular fixed point equation, is one in which a function will map back onto itself for a specific point. Mathematically this means if we have some number a it is a fixed point if and only if:

$$f(a) = a. \tag{3.44}$$

The standard procedure for solving fixed point equations is to choose some initial guess for the variable, find the value at that point and check to see if they match. If they do not match you continue to input the result until the match is found. This take the form:

$$f(x_n) = x_{n+1} \tag{3.45}$$

where n is the current iteration. Convergence of these equations are dependent on 3 different conditions [15]. If I is some closed interval then:

- $x_k \in I$, for each k
- $\lim_{k \rightarrow \infty} x_k = x^*$ where x^* is the solution
- x^* is the only solution in the interval

These conditions mean that in order to get to a solution, there has to exist a solution and that each subsequent iteration must get closer to that solution while staying inside the closed interval. It is important to note that fixed point equations have no built in mechanism to ensure that subsequent iterations stay within the closed interval.

3.3.3.2 Calculating Equilibrium Solutions

For equation 3.43 we are looking for a function $\phi(\mathbf{r})$ that will map back onto itself. Equation 3.43 can be solved using fixed point iteration for $\phi(\mathbf{r})$, which represents the solution for the lowest free energy for a system with potential U_{AB} . This equation has no built in mechanism for keeping $\phi(\mathbf{r})_{n+1}$ between zero and one, which presents a problem since the right hand side of equation 3.43 cannot resolve functions which are not bounded between zero and one because of the logarithmic terms.

A very simplistic solution to his problem is to threshold the resulting density at each iteration so that any value above one and below zero is placed between zero and one. When solving fixed point equations it is important to pick reasonable stopping criteria for the solution. In this case the stopping criteria was chosen to be

$$|(\phi(\mathbf{r})_{n+1} - \phi(\mathbf{r})_n)| \leq \tau k = k_{max} \quad (3.46)$$

which means that the program will stop when the new computed solution differs from the last computed solution by some user chosen amount τ or when the program reaches some maximum number of iterations. There is a subtle problem with the first set of stopping criteria, if we change the value of $\phi(\mathbf{r})_{n+1}$ then it is not warranted to compare it to the previous density in the stopping criteria. This means the threshold procedure needs to be done after the stopping criteria is calculated. However, this threshold means that the stopping criteria will not ever be met since the values being inputted are not the true next iterative step.

We can further get past this limitation by examining systems close to the weak segregation limit, looking at systems that do not fully microphase separate when in equilibrium. This is equivalent to choosing a temperature that is close to the phase transition between a uniform state and the microphase separated state. This condition restricts the possible choices in parameters for the problem, the temperature cannot be lowered too much or the system will not converge properly because of the threshold issue.

For very large disparities in the sizes between the “solvent” molecules and the regular colloids, instead of choosing an initial condition that is random, choosing an initial condition that is closer to a microphase separated structure can result in better convergent properties. Using this along with the threshold technique we are able to get sensible results for some cases.

3.3.3.3 Algorithm

In order to decide the next guess for the algorithm a mixing procedure needs to be decided on. When finding the next iterative input for a fixed point method we can mix the old input with the newly calculated input. The simplest way to achieve this is to take some fraction of the new result to use with the old result. This is called simple mixing and is represented by:

$$\phi(\mathbf{r})_{n+1} = (1 - \rho)\phi(\mathbf{r})_n + \rho\phi(\mathbf{r})_{n+1/2} \quad (3.47)$$

where n is the iterative step and the $\frac{1}{2}$ represents the pure computed density. Using this method increases stability, however ρ is fixed and if chosen poorly, can cause the system to converge slowly or not at all. There exists linear extrapolation methods like Anderson mixing, which have had success in field theory simulations of diblock copolymer melts [45]. Unlike simple mixing, Anderson mixing uses the output of several iterations to calculate the best mixing parameters possible. However, Anderson mixing requires the use of a deviation function to calculate the best new mixing parameter. This strategy is incompatible with the use of a threshold procedure, and as such cannot be used to converge the system more rapidly.

Instead of using Anderson Mixing we use a pseudo variable mixing method in which we use a small mixing parameter initially and measure the rate of convergence. Once the rate goes below a certain value, or a certain number of steps have preceded then the step size is increased temporarily. This improves the convergence rate while not being big enough to cause divergences. The choice of the small and large step size is mostly left up to trial and error. We found through experimentation that using a big step size, 10 times larger than the small step size, was sufficient to speed up convergence.

Now our algorithm proceeds very similarly to the standard SCFT algorithm except there is now only one equation. First we pick a random initial guess for $\phi(\mathbf{r})$

deviated around the global volume fraction (f_A, f_B, \dots) . This initial guess $\phi_0(\mathbf{r})$ is used to calculate $\phi_{\frac{1}{2}}(\mathbf{r})$ where the $\frac{1}{2}$ is used to signify that this is not the final form for the density. We then use $\phi_{\frac{1}{2}}(\mathbf{r})$ and $\phi_0(\mathbf{r})$ to calculate $\phi_1(\mathbf{r})$ using 3.47. If the conditions for termination have not been met then the calculated density needs to be checked to make sure that it does not have elements that go above one or below zero. If it does the result is thresholded correspondingly and the process is continued until the stopping conditions have been met.

Chapter 4

Results and Discussion

4.1 Three Species Case

We look to apply our approach to the situation of 3 different particle species isotropically interacting with one another. The two species case has been covered extensively by von Konigslow *et al.* [23] using the same approach. In the two species case von Konigslow showed that the phases found using our approach matched very closely to the standard SCFT results for diblock copolymers. He found that through varying the volume fraction of one of the particles he could mimic the phase progression seen in diblock copolymers systems. He was able to replicate all the major phases of the diblock system; including the lamella, gyroid and spherical phases [23].

4.1.1 Parameters

Using multiple distinct species increases the amount of total parameters that can be used to specify the system. We focus on the three species case as this is the next simplest case, and further assume that the potentials for the different species have the exact same parameters to reduce the complexity. The parameters that can be specified are:

- The strength of the interactions A_1, A_2
- The length of the repulsive part of the interaction λ
- The set of volume fractions for the system f_A, f_B, f_C with $f_A + f_B + f_C = 1$
- The size of the computational box
- The strength of the incompressibility penalty κ
- The particle size ratio α .

Additionally we have to set the size of the computational box big enough to explore the parameter space freely, as well as set the incompressibility high enough to get a physically meaningful solution. Therefore these are not free parameters as they need to be set to allow for a proper solution.

The interaction strength parameters, A_1, A_2 are chosen to be high enough that the system does not tend toward a uniform state, in which the local volume fractions are equal to the global volume fractions over the space. We can examine what happens to the phases for certain choices of the strength parameters. If for example $A_1 = 1$ and $A_2 = 0$ the potential will effectively be just a repulsive potential between the particles. This means that the system will tend to macrophase separation, in which the A, B and C particles will aggregate together, and any structure will be lost. With the converse, $A_1 = 0$ and $A_2 = 1$ we get a system that will tend to a uniform local volume fraction since the potential is purely attractive between different particles and this will maximize the entropy.

The incompressibility term needs to be chosen to be sufficiently high that the system will converge and obey the incompressibility requirements. The box size will also need to be sufficiently large as to allow for a repeatable micro-structure to form. The initial state for the system was chosen to be a randomly varying about the volume fractions for all of the different particles. Given enough runs the system should converge into all of the possible fixed points, and meta stability can be checked by comparing the free energy of the system to that of a uniform distribution.

The particle size measure was kept to a constant $\alpha = 1$ for all three particles. This was done in order to better compare to results for triblock star polymer melts. We are not looking at a particulate in a solution; so having a large disparity is not an effective way of describing the system.

The main way to vary the different phases will be in adjusting the volume fractions for each of the particles. By creating asymmetries in the system by having more of one particle than the other, the final equilibrium will change to account for this mismatch. We will match the triblock volume fractions used by others in order to compare our approach to theirs.

4.1.2 Relation to Copolymer Melts

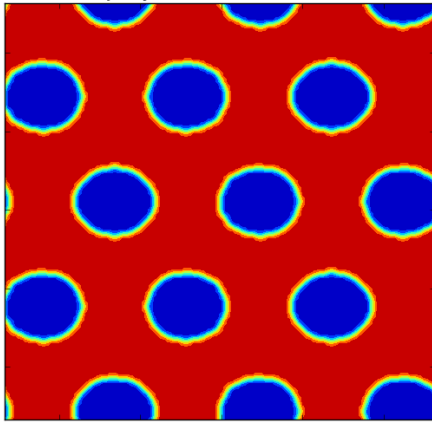
The three species case has many similarities to the case of an ABC triblock copolymer melt. This type of system has been studied before extensively using SCFT with a wide degree of success [17, 42, 54]. There are a large number of examples of this type of system being studied using field theory in two dimensions. We choose to focus our comparisons to the copolymer melt simulations made in two dimensions, since there are more results to compare to. Our approach however is not limited to two dimensional calculations and is in fact easily scalable to studying three dimensional morphologies.

Fredrickson *et al.*, Tang *et al.* and Zhang *et al.* [17, 42, 54], have results using SCFT for ABC miktoarm triblocks in two dimensions and we look to compare the phases they obtain for a certain set of volume fractions to what we can do for the same set of global volume fractions. Since the polymers in a star triblock are all attached at one end, they all feel an interaction due to the other polymers. In a linear triblock this is not true since the polymers are joined end to end. We compare to star polymers since in our approach a specific species of particle interacts with all the other species, which is analogous to what is happening in the star polymers.

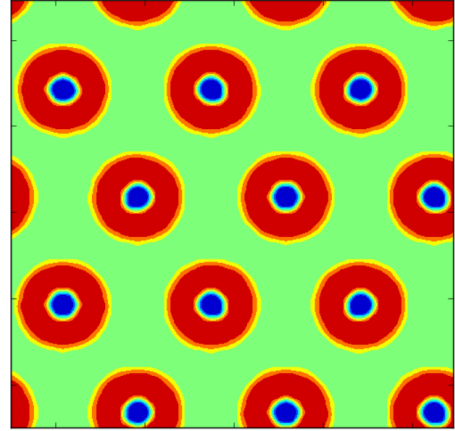
The SCFT model for polymers has the added benefit of using only the Flory-Huggins (χ) parameter to determine the strength of the interaction between two different polymer types. In our case the potential is highly modular, and takes 3 parameters to specify. While keeping the strength of the potential the same it is possible, while adjusting the length scale of the potential, to replicate some of Tang's results. We want to replicate the most robust of the phases found for two dimensional copolymer melt simulations. Since χ is inversely proportional to temperature [17], and the interaction strength for our model is as well, it is natural to fix the potential strength for any comparison.

For figure 4.1, $A_1 = A_2 = 2.8$ is set constant for all runs with a box size $L = 10$, while the volume fractions are changed depending on the phase to be compared to in Tang's results [42]. Only five of the seven results can be replicated with the particle based model, and this is done by manipulating the length scale in the potential, through a trial and error approach. The plots themselves were created using a majority scheme, if the density of a particular particle is above 0.5 then it is considered the majority at that point and is plotted as a single color. Any discolourations in the actual plot itself are regions in which the densities of two particles are roughly equal, and need to be smoothed out. These points are the particle-particle interfaces, where two areas of particles meet. The potential length scale needs to be adjusted between each of the runs.

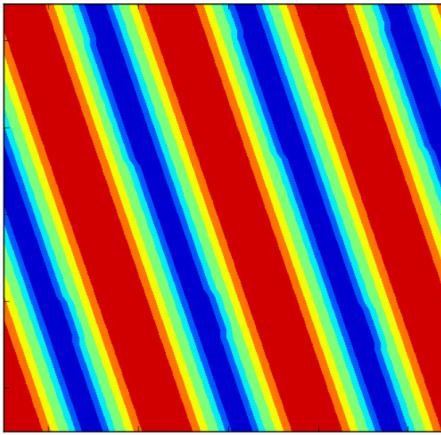
If we consider honeycomb hexagon phase, lamella phase, lamella with beads and octagon-octagon-tetragon phase, to be the most common since these phases appear in all three papers [17, 42, 54], our approach can replicate three of those phases. The octagon-octagon-tetragon phase is the one phase that our approach is unable to replicate. This phase may need the specific connectivity of the polymers in order to form. Since our model deals with particles that interact through a potential instead, it lacks that same type of connectivity. This may be the reason why that specific phase cannot be found as of yet. One way to recreate the tight binding between polymers in our model is to increase the strength of the attractive part of the potential, mimicking the binding of the polymer strands at one end. However making the binding strength of the particles too strong, can cause the system to



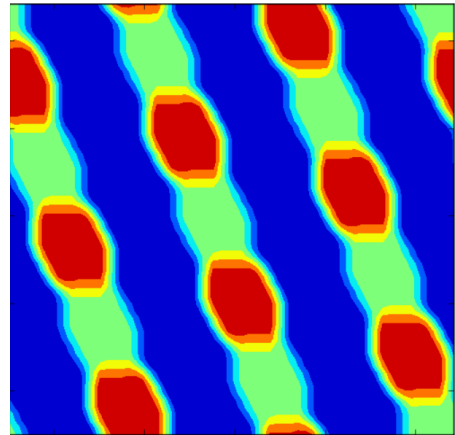
(A) Hexagonal Packed



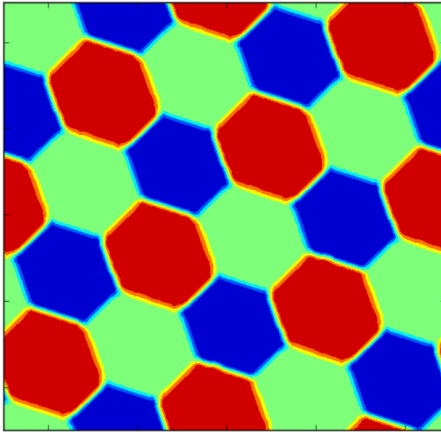
(B) Core Shell



(C) Three Color Lamella



(D) Lamella With Beads



(E) Three Color Hexagonal Honeycomb

FIGURE 4.1: Majority plots for the 5 phases using our model using a grid size of 128 by 128. The figures represent the different particles as a color, If there is more of a particular species at any given point it is assigned a color. Each figure has the following volume fractions f_A, f_B, f_C (a) Hexagonal Lattice Phase (0.8,0.1,0.1) $\lambda = 0.95$ (b) Core-Shell Hexagonal phase (0.1,0.7,0.2) $\lambda = 0.7$ (c) Three Color Lamella (0.5,0.1,0.4) $\lambda = 0.8$ (d) Lamella With Beads Phase (0.6,0.2,0.2) $\lambda = 0.95$ (e) Three color Hexagonal Honeycomb Phase (0.3,0.4,0.3) $\lambda = 0.8$. The last term is the length of the repulsive section of the potential.

become numerically unstable. This problem with increasing A_2 is evident even in the two particle model, where a more clear exploration of the parameter space was made [23]. This is not to say that the the coarse grain particle model cannot get to these phases, it however requires a way to examine this region of the parameter space that is more numerically tractable.

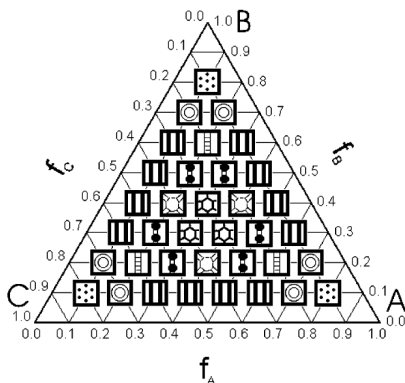




FIGURE 4.2: This is a ternary plot of the volume fractions for an ABC star triblock copolymer melt created by Tang *et al.* [42]. The numbers represent the regions where a certain choice of volume fraction will lead to that phase.

1. Hexagonal Packed  2. Core Shell Hexagonal  3. Three color Lamella  4. Lamella with Beads  5. Knitting Pattern  6.

Octogon-Octogon-Tetragon  7. Honeycomb Hexagon  The kitting phase and the octogon tetragon phase do not appear in our results, instead those areas of the plot is a combination of lamella with beads and lamella phases.

Those two phases are small and the general structure of the plot is recoverable in our approach. Taken from [42]

Figure 4.2 is a ternary plot made up of the volume fractions from Tang’s paper [42]. We wish to note that the larger areas of the plot are recoverable using our approach. The only two phases that cannot be recovered are the more complex phases of the seven that Tang found. Since we are after the most common and robust phases this result does not really interfere with this goal. Figure 4.3 represents the more complex phase diagrams from Zhang *et al.* [54]. Zhang does a more complete search of the center of the phase plot and finds an additional 4 phases in that region, that Tang *et al.* did not find. Notice when comparing the two phase diagrams that in the same areas they find roughly the same phases. Those results correspond to our own results, as we can mimic the broad strokes of these two

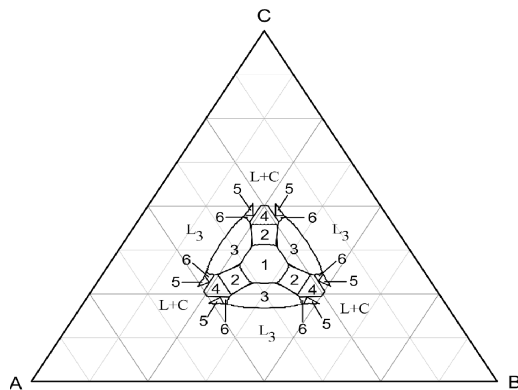


FIGURE 4.3: This is a ternary plot of the volume fractions for a ABC star triblock copolymer melt created by Zhang *et al.* [54]. It is a more specific version of figure 4.2. The more robust phases seem to have the largest areas in the phase plot. This is consistent with our results in which the honeycomb lattice phase, lamella phase and lamella with beads phase take prominence over the other possible phases. The different sections are represented by 1. [6.6.6] 2. [8.6.4;8.6.6] 3. [8.8.4] 4. [10.6.4;10.6.4;10.6.6] 5. [12.6.4] 6. [8.6.4;8.8.4;12.6.4;12.8.4]. The notation [A,B,C] represents the number of connections each polygon makes. For example [6,6,6] means that each polygon is surrounded by 6 other polygons. With more complicated patterns the number of connections can vary depending on pattern. See figure 2.5 for corresponding images. Taken from [54]

phase diagrams. Since we aim to use our approach to find the most common and robust phases a specific search in a region of the phase diagram is outside of the scope of what this approach is for.

4.1.3 Effect of the Length Scale

For the hexagonal honeycomb packed phase $\lambda = 0.8$ was used. If we lower this number the system will become disordered since the potential becomes much closer to a purely attractive potential. If we raise the value of λ to approximately 1.5 we will change the equilibrium structure of the system, to become more like the lamella with beads phase, see figure 4.4. If λ is increased even further we will get a state in which the particles are separated into large aggregate chunks. This is due to the fact that when λ is increased far enough the potential looks mostly repulsive over the domain, which will cause particles alike in type to come closer

together. In manipulating λ we can replicate some of Tang's results but we can also use it to explore different phases as λ is increased.

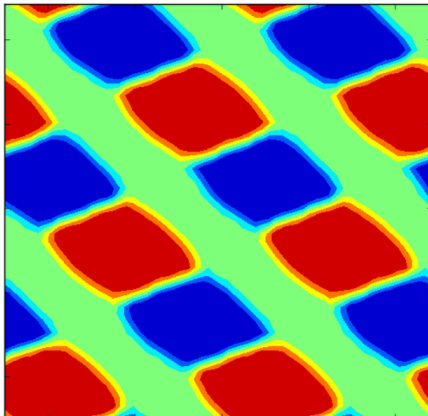


FIGURE 4.4: This is the majority plot for a lamella with beads plot. This plot was obtained by keeping the volume fractions for a hexagonal honeycomb phase (0.3,0.4,0.3) and increasing the value of λ to 1.5. Changing the length scale will change the final equilibrium structure. Tang's results are repeatable in our approach for only a small subset of the length, which is due to increased complexity of our interaction.

Our model is highly dependent on the length scale of the potential. Through simple adjustment of the length scale the morphology of the system completely changes. This spatial extent adds complexity, allowing us to examine a larger phase space of possible solutions. Adjusting the potential length scale to match the polymer results is justified in the following way; while polymers have actual spatial extent our particles are effective point particles that interact spatially. It is in this way one can compare the two models, as they both have some sort of long range interaction, one through the physical length and one through the interaction potential. The length of the potential, in the polymer model, does not have an explicit value like it is in our model. This gives us the ability to examine the effect of an extra parameter on the final local volume fraction in the system.

Otherwise the only values that are changed between the different runs are the global volume fractions of the different particles. The differences between the particle model and the miktoarm polymer model, is that the polymers are all attached at one end. This is an architectural restriction on the polymers themselves that

our particle system does not inherently have. This may be the reason as to why our model cannot replicate the knitting pattern, and the octagon-octagon-tetragon phase.

Looking at the work of others who examine triblock star polymers we find a wide degree of different phases can be found [10, 17, 42, 54]. It is important to note that in some cases the phases that are found do not match up completely but there are a set of phases that appear in all the works. Phases such as the honeycomb lattice phase and the lamella phase appear consistently, in the literature and also in our own work. It gives evidence that the phases found by our approach are the ones that are the most robust and easiest to find in the parameter space. It is easy to see that we could just use the standard SCFT approach for triblock copolymers, but we want to focus on a method that has a high throughput. A strategy that has been outlined by both Xu *et al.* [53] and Matsen *et al.* [30] is using a combination of fast algorithms and novel initializations we can explore even more of the parameter space for potential morphologies. Using a variety of different initialization procedures instead of just using random distributions as the initial input, Xu states that this will allow us to explore even more potential phases. Our approach, at least for two dimensions, can very quickly and simply get out the robust phases and if needed a more accurate, but slower model, can be used for more complicated phases. Our approach is well suited to being an important part of an algorithm that can explore the stable and metastable morphologies for a wide degree of parameters and initial inputs.

4.1.4 Three Dimensional Phases

We focused on the existence of morphologies in two dimensions but the extension to three dimensions is straightforward. Many interesting three dimensional morphologies are easily obtainable. We choose not to focus on benchmarking this approach in three dimensions since the results for SCFT for three dimensional star triblock copolymer melts are sparse. As such figure 4.5 represents some of the simpler phases found in three dimensions.

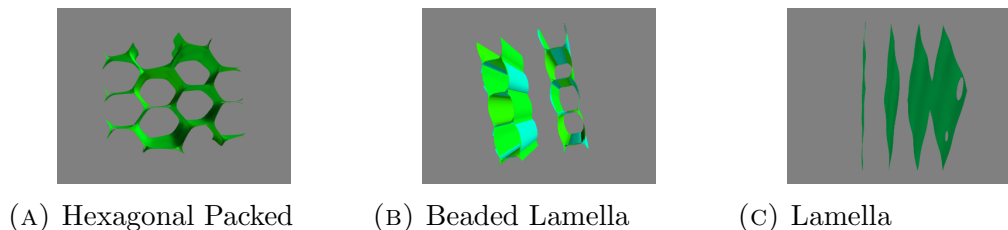


FIGURE 4.5: This is an isosurface plot (the surfaces enclose volumes where each particle is represented at a majority) for a hexagonal phase in 3 dimensions with a box size of $L = 6$. This plot was obtained by keeping the volume fractions (f_A, f_B, f_C) for each plot at A) $(0.33, 0.33, 0.33)$ and $\lambda = 1.5$. B) $(0.46, 0.27, 0.27)$ $\lambda = 1.6$ C) $(0.2, 0.4, 0.4)$ $\lambda = 1.6$.

Figures 4.5 were generated by looking at the work done by Fredrickson [17] for two dimensional phases. Using the same volume fractions as the two dimensional phases we can assume that a similar structure will exist in three dimensions, by stacking the two dimensional results. Unlike some of the other simulations that involve particles interacting isotropically [3, 4] our approach is easily scaled to three dimensions. We have the equivalent to the honeycomb hexagon phase, the lamella with beads phase and lamella phase in three dimensions. In comparison to the three dimensional results from Xu *et al.* [53] we find that Xu was able to also get these phases for a star triblock copolymer.

4.1.5 Improvements and Future Work for Polymer Systems

The main drawback of using the coarse grain particle approach on polymer systems is it does not capture all the properties of the polymer system. There are still phases that cannot be found using this approach, though it may still be possible using a slightly different potential to replicate the knitting pattern, and octagon-octagon-tetragon phase. Also we kept the potential for each of the particles the same to lower the complexity and to compare with polymer results that have the χ parameter the same for all parameters. However, there exists many situations in triblock polymers where this is not true, and this approach could also be verified against those types of systems. The paper by Xu *et al.* [53] indicates that there is merit in possibly using a wide variety of initial conditions to study the possible

morphologies. The runs done in our approach used random initial conditions. It is possible that the use of more specific initial conditions will yield the more complex results from the papers by Tang *et al.* and Zhang *et al.* [42, 54].

This approach still needs to be benchmarked more thoroughly for three dimensional morphologies of triblock copolymers. The results for three dimensional triblocks are not as plentiful as their two dimensional counterparts but there are still cases that can be compared to [37, 40, 53]. This is an important next step in seeing how this coarse grain particle approach works with polymer systems. Also this approach needs to be modified so that it can be benchmarked against linear triblock copolymers. Tang *et al.* also have a series of SCFT solutions to a system of linear ABC triblocks [41], which gives a solid benchmark to compare to.

There is also no restriction on increasing the number of particles in the model to mimic high block copolymer systems. There exist simulations for two dimensional 4-block copolymers [50], and our approach could be benchmarked against the common robust phases for that type of system as well.

4.2 Particle Disparity

Using the standard SCFT equations 3.29 there is a computational limit to how far the particle size measure can be lowered. When looking at the effect of solvent molecules when interacting with diblock copolymers in traditional SCFT it has been shown that looking at a particle disparity of less than $\alpha = 0.01$ causes numerical instability [25]. For our system in the standard SCFT implementation, a disparity limit of $\alpha = 0.01$ was also reached [23]. As the particle size is decreased the entropy dominates and as a result the temperature needs to be decreased for any microphase structures to form [23]. This results in the step size having to be decreased in order to get convergence, which for extreme cases of the particle size difference, the system would never converge. In order to look at systems with lower levels of particle disparity, the DFT like equations (equation 3.43) are necessary,

as the scaling of the exponential due to particle size has been removed by framing the problem in terms of logarithms.

Getting down to much smaller α requires a more careful procedure, which we have outlined. We aim to bring the size disparity of the particles to $\alpha = 10^{-6}$, which simulates the natural size difference between a nano-colloid and the solution that it is suspended in. Using our model we had some success in 1D and 2D simulations of this system. The sharp temperature cutoff, the temperature where the system goes from disordered to ordered is troublesome for our method. The translational entropy terms in the free energy are each weighted by the inverse of their respective α terms, which means when the particle size is very small these terms dominate the free energy. This makes the system much more favorable to a disordered state at high temperatures, as one would expect. The decrease in particle size, for one of the particles, amounts to being able to fit more particles in the same amount of space as the other species.

4.2.1 Two Different Sized Particles in 1D

For one dimensional systems we were able to get a convergent solution to our free energy minimum. The sharp temperature cut off for a weakly segregated system still exists but that phase is observable for some choice of the A_1 and A_2 parameters. Depending on the choice of the particle size α , we have found that the choice of the κ term, that maintains proper volume fractions, needs to be at least $100 \times \alpha^{-1}$ in magnitude. Choosing this term to be too small will result in the volume fractions not being conserved in the final solution.

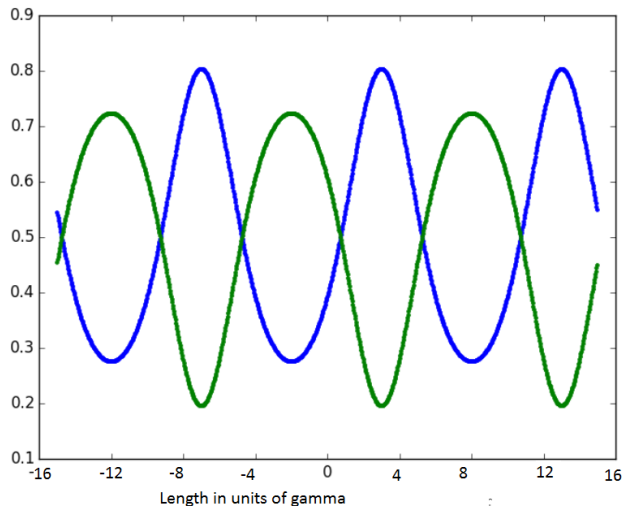


FIGURE 4.6: This is a plot of the 2 particle case, with 1024 computation points. The blue line represents the solvent and the green line represents the larger particle. In this case the size of one of the particles is much smaller than the other. The y-axis represents the volume fraction of a particle at a particular point. This is a much more realistic size ratio between a colloid and a particle in a solution $\frac{v_B}{v_A} = 10^{-6}$. A_1 and $A_2 = 0.36$

The results in figure 4.6 are what one would expect when one of the particles is much smaller than the other. Realistically one does not expect that any one portion of the box will contain only one particle. The smaller particles will always be able to mix, to some degree, with the larger particles and this is represented here. Even though mean field theory obscures any information about detailed packing structure, we can still use it to recover some large scale detail of the underlying structure. The decrease in size of one of the particles also has the effect of increasing the strength of the interaction in order to counter the entropic gains of a smaller particle size.

4.2.2 Two Different Sized Particles in 2D

The two dimensional case is much more difficult to get accurate solutions of equation 3.43 with the right level of size difference between the particles. In the one dimensional case we were able to fine tune the strength of the interaction to get to the weakly segregated limit. This strategy avoids the use of continuously having

to threshold the outputs after they have been compared which can lead to a continuous loop. The problem encountered in 2D is that the boundary from weakly segregated system and a system which cannot be resolved with this algorithm may be very small. Meaning that at some point increasing the strength by even a tiny amount will result in a system that diverges due to the threshold scheme.

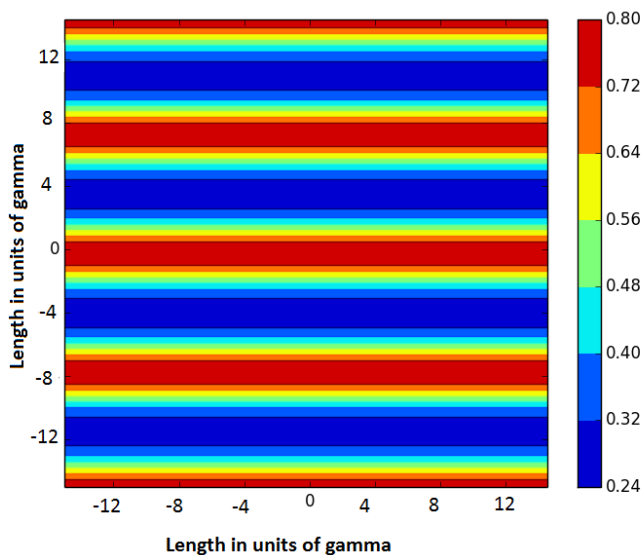


FIGURE 4.7: This is a plot of the 2 particle case, in which a single local volume fraction for one of the particles is plotted on a 64 by 64 grid. In this case the size of one of the particles is much smaller than in the other case. This is a much more realistic size ratio between a colloid and a particle in a solution $\frac{\alpha_B}{\alpha_A} = 10^{-6}$. The scale represents the amount of any given particle in a particular region.

The only obtainable microstructure with this particle size was a lamella type morphology, figure 4.7. Using $A_1 = A_2 = 0.035$, $\lambda = 4$, and $\gamma = 1.0$, we are able to obtain a structure that exhibits an interesting microstructure. One of the issues with this method is the need to specify an initial condition that is not going to be a random seed. A structure that already exhibits lamella properties is used as the initial input. The temperature is then adjusted around the order-disorder transition, to find a structure in the weak segregation limit. Using a non-random initial input, allows us to get closer to the solution allowing the system to converge without going into a threshold loop.

Just like the one dimensional case the structure reflects the fact that one of particles is much smaller than the other. From the scale in figure 4.7, the maximum amount of the larger particle is about 0.8, and since incompressibility is strictly enforced, the smaller particle takes up the rest of the space. The density for the larger particles never reaches the maximum, reflecting that smaller particles will be able to fit in between larger ones. This is a good check that the model replicates this in one and two dimensions, as this is what is expected to happen in reality.

4.2.3 Convergence

Choice of the potential parameters becomes increasingly difficult due to the large parameter space of the system. Since the potential strength is tied inversely to the temperature, lowering the temperature is equivalent to raising the strength. In general when lowering α and then choosing the strength to be high the system will not converge to a final solution. This is due to the problem mentioned previously, the values that can be imputed into equation 3.43 have to be bounded between 0 and 1. However the values that are outputted do not have to be bounded, thus the outputs need to be put under some sort of threshold in order to be used in the fixed point equation. This happens when the temperature is lowered, however, it is at lower temperatures where you expect that the system will be able to self assemble. Choosing too high of a temperature results in a divergence that will never get below a certain value. Raising the value of A_1, A_2 above 0.36 results in a divergent system, at this point the threshold starts to become a factor and the system will never converge.

If it is a matter of choosing the right system parameters to get a meaningful result, a parameter space search would be a good starting point. The problem being that just considering the potential itself, there are 3 parameters that need to be set. This is already a large parameter space to explore. We explored the parameter space of the potential using a computing cluster, with no results for phases other than lamella. A brute force approach to finding the right set of parameters will not work.

This issue was not inherently present in the SCFT equations due to the self limiting nature of the exponentials that determined the densities. Using the logarithmic form of the equations removed this inherent property of the SCFT equations. In using an equation that can handle the numeric problems of lowering the α parameter we have inherently introduced a new problem of being unable to resolve solutions for a larger number of different parameter sets.

4.2.4 Improvements and Future Work for Particle Disparity

Inability to freely explore the parameter space using this DFT like model is a hindrance to its usefulness for studying particle disparity effects. The most prominent issue is that the fixed point method can give outputs that cannot be used as inputs in the fixed point equation. Even in the two dimensional case some knowledge of the end phase is needed in order to use get a useful equilibrium solution. Having a method that has a way to use bounded inputs that does not result in an infinite loop, is one area that can see improvement.

Three dimensional results are of the utmost interest because of the real world comparisons that can be made. Being able to explore the parameter space in three dimensions is one area of interest. Getting the current model to work in three dimensions is challenging, with the parameter restrictions that are present in two dimensions being even more pronounced. The methods used in 1D and 2D do not carry over explicitly in 3D, so new ideas will have to come into play.

The use of high performance computing may be able to make up some of the difference. If it is a matter of choosing the right potential parameters in order to get a convergent and meaningful result, being to explore a large amount of the parameter space might provide some insight. The total number of parameters is quite high, so some sort of reduction of the total parameters is needed in order to narrow the search field, or to discover what are the most important parameters in the system.

Chapter 5

Conclusions

We have found some success using a system of interacting particles to examine a variety of different soft matter systems. Using particles that interact with short range repulsive and long range attraction, we were able to replicate some of the different phases found in ABC triblock miktoarm copolymer systems. By keeping the particle size constant as well as the potential the same between all of the particles we can go through some of the different triblock phases by varying the volume fractions as well as one of the length scales of the potential.

Of the seven available phases found by Tang we have been able to replicate at least five of those phases. In the more thorough search of the phase space by Zhang *et al.* four more phases were found that are more complicated but the phases that are the most common among star triblock copolymer studies were also found. Those phases were the hexagonal lattice phase, core shell hexagonal phases, three color honeycomb hexagonal phase, three color lamella phase and lamella with beads phase. The two phases that have not occurred in our model, knitting pattern and octagon-octagon-tetragon phase, may be out of reach simply because the miktoarm system has extra restriction due to the fact they are attached at one end. The most robust of the phases are recoverable using our approach, and match up well with other findings for ABC star triblock copolymers systems. We adhere to the idea that this approach can be used to find many different equilibrium phases quickly, and can be used as a launching point for finding more complicated structures.

With modifications to the SCFT equations we were able to explore systems in which the size difference between two particles was at least greater than it was before. There was some success in one and two dimensions, finding the lamella phase for both those dimensions. We were able to show that some features of a system with a realistic size disparity such as the inability for the system to fully separate. Divergence due to functional properties of the fixed point equation in 2D result in concessions having to be made on calculating equilibrium densities. The use of a pre-determined initial condition as well as only being able to explore the weak segregation limit are problems that still need to be resolved. Difficulties in finding solutions in three dimensions persist due to the nature of the modified equations, and work still needs to be done on creating a more successful approach when dealing with particle disparity.

We have used this approach to explore the robust phases of different types of soft matter systems, copolymer melts and colloidal solutions. This method is quick and efficient; and can find the robust phases using an easily characterized potential. This approach in conjunction with more complicated models can be used to find even more complicated phases and construct more accurate phase diagrams.

Appendix A

Appendix A. *Functional Integration*

A functional is a generalization of the idea of a function. Instead of a real or complex number as the argument, a functional takes as its argument a function and returns a number for each function for which the functional is defined. For example a functional can take the form:

$$I[f(x)] = \int_b^a f(x)dx \quad (\text{A.1})$$

The solution to this equation, if it exists, is the value associated for the chosen function $f(x)$. The functional can be thought of as the limit in which the number of variables of the function becomes infinite.

Functional integration is analogous to the regular integration of functions. For standard integration we have some function $f(x, y)$ and the integral of such a function is $\int f(x, y)dxdy$. The function is taken over every point and multiplied by the discrete volume at each step. In functional integration we instead have a set of functions S and a functional F is evaluated at every point and multiplied by a measure of the ‘volume’ of the function space [8].

In principle the set of functions that are being integrated over are infinite dimensional, with an infinite number of variables needed to parametrize the problem. This is obviously not a tractable method practically and thus we replace the functional with a multiple variable function and do a multi variable integration over these variable. In the limit of an infinite number of variables this method should be equivalent to the functional integral [8].

To further illustrate this, we look at an example outlined by J. J. Binney [8]. We wish to integrate the functional:

$$A[f] = \exp \left[-k \int_{-\frac{L}{2}}^{\frac{L}{2}} f^2 dx \right]. \quad (\text{A.2})$$

The functional integral takes the form of:

$$K = \int \mathcal{D}f \exp \left[-k \int_{-\frac{L}{2}}^{\frac{L}{2}} f^2 dx \right]. \quad (\text{A.3})$$

where $\mathcal{D}f$ means integration over all possible values of f . First let us note that:

$$\lim_{n \rightarrow \infty} \exp \left[-\frac{kL}{n} \sum_{i=1}^n f_i^2 dx \right] = A[f]. \quad (\text{A.4})$$

We can then replace the sum over all functions with a regular integral over the variable f_i

$$K_n = \int df_1 \dots df_n \exp \left[-\frac{kL}{n} \sum_{i=1}^n f_i^2 dx \right]. \quad (\text{A.5})$$

solving for K exactly we get:

$$K_n = \left(\frac{\pi n}{kL} \right)^{n/2} \quad (\text{A.6})$$

Conclusions.

since K is equal to K_n as $n \rightarrow \infty$. K_n is divergent in the limit $n \rightarrow \infty$; a normalization factor needs to be used to make the limit exist. However a different normalization needs to be used for each factor of k . This means that functional integration needs to have a different normalization for each functional in order for the answer to be finite. This is not the same as the case for a regular function integration.

In essence this means that functional integration is only useful if the number of functions that can be used are finite. This property is apparent in physical problems such as the integration of the partition function, in which the Hamiltonian is dependent on a function. The physically realizable set of functions can be used as the integration space, meaning a functional integral can be performed meaningfully.

Bibliography

- [1] Pinar Akcora, Hongjun Liu, Sanat K. Kumar, Joseph Moll, Yu Li, Brian C. Benicewicz, Linda S. Schadler, Devrim Acehan, Athanassios Z. Panagiotopoulos, Victor Pryamitsyn, Venkat Ganesan, Jan Ilavsky, Pappanan Thiyagarajan, Ralph H. Colby, and Jack F. Douglas. Anisotropic self-assembly of spherical polymer-grafted nanoparticles. *Nature Materials*, 8(4):3549, April 2009.
- [2] A. Alivisatos, Paul Johnsson, Kai P. Peng, Xiaogang Wilson, Troy E. Loweth, Colin J. Bruchez, Marcel P. Schultz, Peter G. Organization of ‘nanocrystal molecules’ using DNA. *Nature*, 382(6592), 609-611, August 1996.
- [3] A J Archer, C Ionescu, D Pini and L Reatto. Theory for the phase behaviour of a colloidal fluid with competing interactions. *J. Phys. Condens. Matter*, 20(41), 415106, 2008.
- [4] Andrew J. Archer Two-dimensional fluid with competing interactions exhibiting microphase separation: Theory for bulk and interfacial properties, *Physical Review*, 78(3), 2008.
- [5] Ashok Das. Field Theory: A Path Integral Approach. *World Scientific*, London, 1993.
- [6] Emanuela Bianchi, Christos N. Likos, and Gerhard Kahl. Tunable Assembly of Heterogeneously Charged Colloids. *Nano Letters*, 14(6), 3412-3418, 2014
- [7] Paul L. Biancaniello, Anthony J. Kim, and John C. Crocker. Colloidal Interactions and Self-Assembly Using DNA Hybridization. *Physical Review Letters*, 94(5), 058302, 2005.

- [8] J. J. Binney, N. J. Dowrick, A. J. Fisher and M. E. J. Newman. The Theory of Critical Phenomena: An Introduction to the Renormalization Group. *Oxford University Press*, New York, 1999.
- [9] S V Buldyrev, G Malescio, C A Angell, N Giovambattista, S Prestipino, F Saija, H E Stanley and L Xu. Unusual phase behavior of one-component systems with two-scale isotropic interactions. *Journal of Physics: Condensed Matter*, 21(50), 2009.
- [10] Xuguang Cao, Liangshun Zhang, Liquan Wang and Jiaping Lin. Insights into ordered microstructures and ordering mechanisms of ABC star terpolymers by integrating dynamic self-consistent field theory and variable cell shape methods. *Soft Matter*, 10(32), 5916-5927, 2014.
- [11] J. C. Crocker, Three-dimensional nanoparticle arrays are likely to be the foundation of future optical and electronic materials. A promising way to assemble them is through the transient pairings of complementary DNA strands. *Nature*, 451(7178), 528-529, 2008.
- [12] Remi Dreyfus, Mirjam E. Leunissen, Roujie Sha, Alexei Tkachenko, Nadrian C. Man, David J. Pine, and Paul M. Chaikin. Aggregation-disaggregation transition of DNA-coated colloids: Experiments and theory. *Physical Review*, 81(4):110, April 2010.
- [13] Duhamel P, Vetterli M. Fast Fourier Transforms: a Tutorial Review and a State of the Art. *Signal Processing*, 192, 9-299, 1990.
- [14] S. F. Edwards. The statistical mechanics of polymers with excluded volume. *Proceedings of the Physical Society*, 85(4), 613, , April 1965.
- [15] L. Elden, L. Wittmeyer-Koch, and H. B. Nielsen. Introduction to Numerical Computation - analysis and Matlab illustrations. *Student literature*, Lund jul 2004.
- [16] J. G. E. M. Fraaije and G. J. A. Sevink. Model for Pattern Formation in Polymer Surfactant Nanodroplets. *Macromolecules*, 36(21), 78917893 , 2003.

- [17] Glenn H. Fredrickson, Venkat Ganesan and François Drolet. Field-Theoretic computer Simulation Methods for Polymers and Complex Fluids. *Macromolecules*, 35(1):1639, January 2002.
- [18] Daan Frenkel, David J. Wales. Colloidal self-assembly: Designed to yield. *Nature Materials*, 10(6), 410411, 2011
- [19] Dmytro Nykypanchuk, Mathew M. Maye ,Daniel van der Lelie, Oleg Gang. DNA-guided crystallization of colloidal nanoparticles. *Nature*, 451(31), 549-552, 2008.
- [20] Dmytro Nykypanchuk, Mathew M. Maye ,Daniel van der Lelie, Oleg Gang. Binary Heterogeneous Superlattices Assembled from Quantum Dots and Gold Nanoparticles with DNA. *Nature*, 451(31), 549-552, 2008.
- [21] Eugene Helfand. Theory of inhomogeneous polymers: Fundamentals of the Gaussian random-walk model. *The Journal of Chemical Physics*, 62(3), 1975.
- [22] Johan Skule Høye, Enrique Lomba and Noé Garcia Almaraz. One- and three-dimensional lattice models with two repulsive ranges: simple systems with complex phase behaviour. *Molecular Physics*, 107(20) 46, 2009.
- [23] K von Konigslow , E D Cardenas-Mendez , R B Thompson and K O Rasmussen. The self-assembly of particles with isotropic interactions. *Journal Of Physics: Condensed Matter*, 85(4):613624, April 2013
- [24] Z. Y. Tang, N. A. Kotov. One-dimensional assemblies of nanoparticles: preparation, properties, and promise. *Advanced Materials*, 17, 951962 2005.
- [25] Li, W. and Jiang, W. Effect of Solvent Molecular Size on the Self-Assembly of Amphiphilic Diblock Copolymer in Selective Solvent *Macromolecule. Theory Simulation.*, 18(16) 434-440, 2009.
- [26] Weihua Li, Yuci Xu, Guojie Zhang, Feng Qiu, Yuliang Yang, and An-Chang Shi. Real-space self-consistent mean-field theory study of ABC star triblock copolymers, *The Journal of Chemical Physics*, 133(6), 2010.

- [27] Y. Y. Pinto. Sequence-encoded self-assembly of multiple-nanocomponent arrays by 2D DNA scaffolding. *Nano Letters.*, 5(2), 23992402, 2005.
- [28] Francisco Martinez-Veracoechea, Bianca Mladek, Alexei Tkachenko, and Daan Frenkel. Design Rule for Colloidal Crystals of DNA-Functionalized Particles. *Physical Review Letters*, 107(4):1013, July 2011.
- [29] M. W. Matsen, and M. Schick. Stable and unstable phases of a diblock copolymer melt *Physical Review Letters*, 72(16): 2660-2663, 1994. American Physical Society
- [30] Mark W. Matsen. New Fast SCFT Algorithm Applied to Binary Diblock Copolymer/Homopolymer Blends. *Macromolecules*, 36(25):96479657, 2003.
- [31] Mark W. Matsen. The standard Gaussian model for block copolymer melts. *Journal of Physics: Condensed Matter*, 14(2):R21R47, January 2002.
- [32] Lorenzo Di Michele and Erika Eiser. Developments in understanding and controlling self assembly of DNA-functionalized colloids. *Physical Chemistry Chemical Physics*, 15(9) , 31152013, 2013.
- [33] Lorenzo Di Michele, Francesco Varrato, Jurij Kotar, Simon H. Nathan, Giuseppe Foffi, Erika Eiser. Multistep kinetic self-assembly of DNA-coated colloids. *Nature Communications*, 4:2007, February 2013.
- [34] C. A. Mirkin, R. L. Letsinger, R. C. Mucic and J. J. Storhoff, A DNA-based method for rationally assembling nanoparticles into macroscopic materials. *Nature*, 382(6592): 607609, 1996
- [35] Robert J. Macfarlane, Byeongdu Lee, Haley D. Hill, Andrew J. Senesi, Soenke Seifert, and Chad A. Mirkin, Assembly and organization processes in DNA-directed colloidal crystallization. *Proceedings of the National Academy of Sciences*, 106(26): 1049310498, 2009.
- [36] Kardar, Mehran. Statistical Physics of Fields. *Cambridge*, 2007.

- [37] K. O. Rasmussen, G. Kalosakas. Improved Numerical Algorithm for Exploring Block Copolymers Mesophases. *Journal of Polymer Science*, 40:1777-1783, 2002.
- [38] L. E. Reichl. Modern Course in Statistical Physics. *University of Texas Press*, 1980.
- [39] W. Benjamin Rogers and John C. Crocker. Direct measurements of DNA-mediated colloidal interactions and their quantitative modeling. *Proceedings of the National Academy of Sciences*, 108(38):1568715692, 2011.
- [40] Mingzhu Sun, Peng Wang, Feng Qiu, Ping Tang, Hongdong Zhang, and Yuliang Yang. Morphology and phase diagram of ABC linear triblock copolymers: Parallel real-space self-consistent-field-theory simulation. *Physical Review* 77: 016701, 2008.
- [41] Ping Tang, Feng Qiu, Hongdong Zhang, and Yuliang Yang. Morphology and phase diagram of complex block copolymers: ABC linear triblock copolymers. *American Physical Society, Physical Review*, 69: 021404, 2004.
- [42] Ping Tang, Feng Qiu, Hongdong Zhang, and Yuliang Yang. Morphology and Phase Diagram of Complex Block Copolymers: ABC Star Triblock Copolymers. *American Physical Society, Physical Review*, 69: 031803, 2004.
- [43] Simon H. Tindemans and Bela M. Mulder. Designing colloidal ground-state patterns using short-range isotropic interactions. *Physical Review*, 137: 021404, 2010.
- [44] R. B. Thompson. Predicting nonpolymeric materials structure with real-space self-consistent field theory. *Physical Review*, 74: 04150118, 2006.
- [45] R. B. Thompson and K. O. Rasmussen, and T. Lookman. Improved convergence in block copolymer self-consistent field theory by Anderson mixing. *The Journal of Chemical Physics*, 120: 31-34, 2004.

- [46] R.B. Thompson, S.Dion, K. Von Konigslow. The Self-Assembly of Particles with Isotropic Interactions Using DNA Coated Colloids to Create Designer Nanomaterials. *AIP Conference Proceedings*, 1590: 229-233, 2014 <http://dx.doi.org/10.1063/1.4870223>
- [47] Panagiotis E. Theodorakis, Christoph Dellago, and Gerhard Kahl. A coarse-grained model for DNA-functionalized spherical colloids, revisited: Effective pair potential from parallel replica simulations. *Journal of Chemical Physics* 138: 025101, 2013.
- [48] Patrick Varilly ,Stefano Angioletti-Uberti, Bortolo M. Mognetti, and Daan Frenkel. A general theory of DNA-mediated and other valence-limited colloidal interactions. *The Journal of Chemical Physics*, 137: 094108 2012
- [49] J. D. Watson and F. H. C. Crick. Molecular Structure of Nucleic Acids: A Structure for Deoxyribose Nucleic Acid. *Nature*, 171(4356):737738, 1953.
- [50] Rong Wang, Tingting Xu. Theoretical study on morphology of ABCD 4-miktoarm star block copolymer. *Polymer* 48(15):4601-4608 2007.
- [51] Qiang Wang and Yuhua Yin. Fast off-lattice Monte Carlo simulations with “soft” repulsive potentials. *The Journal of Chemical Physics* 130:104903 ,2009.
- [52] Kun-Ta Wua, Lang Feng, Ruojie Sha, Remi Dreyfus, Alexander Y. Grosberg, Nadrian C. Seeman, and Paul M. Chaikin. Polygamous particles. *Proceedings of the National Academy of Sciences*, 109(46):18731-18736, 2012. doi: 10.1073/pnas.1207356109.
- [53] Weiquan Xu, Kai Jiang, Pingwen Zhang, and An-Chang Shi. A Strategy to Explore Stable and Metastable Ordered Phases of Block Copolymers. *Journal of Chemical Physics* 117(17):52965305 2013.
- [54] Guojie Zhang, Feng Qiu, Hongdong Zhang, and Yuliang Yang. SCFT Study of Tiling Patterns in ABC Star Terpolymers. *Macromolecules* 43(6):29812989, 2010.